Recurrent, Activating Variants in the Receptor Tyrosine Kinase *DDR2* Cause Warburg-Cinotti Syndrome

Linda Xu,[1,2,3] Hanne Jensen,[4,13] Jennifer J. Johnston,[5,13] Emilio Di Maria,[6] Katja Kloth,[7] Ileana Cristea,[1,2,3] Julie C. Sapp,[5] Thomas N. Darling,[8] Laryssa A. Huryn,[9] Lisbeth Tranebjærg,[10,11] Elisa Cinotti,[12] Christian Kubisch,[7] Eyvind Rødahl,[1,3] Ove Bruland,[2] Leslie G. Biesecker,[5,13] Gunnar Houge,[2,13,*] and Cecilie Bredrup[1,2,3,13]

We have investigated a distinct disorder with progressive corneal neovascularization, keloid formation, chronic skin ulcers, wasting of subcutaneous tissue, flexion contractures of the fingers, and acro-osteolysis. In six affected individuals from four families, we found one of two recurrent variants in discoidin domain receptor tyrosine kinase 2 (*DDR2*): c.1829T>C (p.Leu610Pro) or c.2219A>G (p.Tyr740Cys). *DDR2* encodes a collagen-responsive receptor tyrosine kinase that regulates connective-tissue formation. In three of the families, affected individuals comprise singleton adult individuals, and parental samples were not available for verification of the *de novo* occurrence of the *DDR2* variants. In the fourth family, a mother and two of her children were affected, and the c.2219A>G missense variant was proven to be *de novo* in the mother. Phosphorylation of DDR2 was increased in fibroblasts from affected individuals, suggesting reduced receptor autoinhibition and ligand-independent kinase activation. Evidence for activation of other growth-regulatory signaling pathways was not found. Finally, we found that the protein kinase inhibitor dasatinib prevented DDR2 autophosphorylation in fibroblasts, suggesting an approach to treatment. We propose this progressive, fibrotic condition should be designated as Warburg-Cinotti syndrome.

In 2006, Warburg et al. described an apparently distinct connective-tissue disorder characterized by blepharophimosis, progressive corneal vascularization, retinal dystrophy, conductive hearing loss, acro-osteolysis, and wasting of subcutaneous tissue in the face, hands, and feet.[1] For updated pictures of the described individual, see Figure 1. Cinotti et al. later reported an individual with similar features.[2] In this report we extend the clinical description by identifying four additional individuals, three of whom are from a single family, and identify the molecular cause of this syndrome.

Informed consent was obtained for participation and publication of clinical photographs. The study was approved by the Regional Committee for Medical and Health Research Ethics, Western Norway (IRB no. 00001872, project number 2014/59). The NIH study was reviewed and approved by the National Human Genome Research Institute institutional review board, protocol 10-HG-0065.

The clinical findings are illustrated in Figures 1 and 2 and are summarized in Tables 1 and S1. Pedigrees are provided in Supplemental Figures S1–S4. Individuals 1 and 2 have been described in detail.[1,2] The proband of the third pedigree (individual 3) is a 31-year-old female with two affected children (Figures 2 and S3). She was born with a clubfoot, which was successfully treated. When she was 5 years old, the first red, linear, and firm keloid-like plaque appeared spontaneously on her left forearm. This was slowly progressive. Over the years, several additional red papules and linear or annular plaques developed on her arms and feet, without preceding trauma or inflammation. In contrast, no keloid formations have occurred after surgical and traumatic wounds, with the exception of one instance after an ear helix piercing. At age 14, finger flexion contractures, preceded by painless, non-erythematous swelling of the involved joints, developed. This progressed to ankylosis of proximal interphalangeal (PIP) joints and cutaneous fusion between the digits and the palm (Figures 2E and 2F). Surgical correction and collagenase injections allowed the fixated digit to extend, but rapid recurrence and progression occurred. Gradual cutaneous fusion of the toes led to little or no separation of the toes (Figures 2I and 2J). She has had numerous sterile abscesses of the hands and feet, and these abscesses were often followed by scarring, cutaneous fusions, and contractures. From the age of 25, she developed corneal neovascularization and subsequent pannus and symblepharon formation on the right eye; eventually, there was complete

[1]Department of Ophthalmology, Haukeland University Hospital, N-5021 Bergen, Norway; [2]Department of Medical Genetics, Haukeland University Hospital, N-5021 Bergen, Norway; [3]Department of Clinical Medicine, University of Bergen, N-5021 Bergen, Norway; [4]Eye Department Glostrup Hospital, Rigshospitalet, the Kennedy Centre, DK 2600 Glostrup, Denmark; [5]National Human Genome Research Institute, National Institutes of Health, Bethesda, MD 20892, US; [6]Department of Health Sciences, Division of Medical Genetics, University of Genova, Galliera Hospital, 16128 Genova, Italy; [7]Institute of Human Genetics, University Medical Center Hamburg-Eppendorf, 20246 Hamburg, Germany; [8]Uniformed Services University of the Health Sciences, Bethesda, MD 20814, US; [9]National Eye Institute, National Institutes of Health, Bethesda, MD 20892, US; [10]Department of Clinical Genetics, The Kennedy Center, Copenhagen University Hospital, DK-2200 Copenhagen, Denmark; [11]Institute of Clinical Medicine, University of Copenhagen, DK-2200 Copenhagen, Denmark; [12]Department of Medical, Surgical and Neuro-Sciences, Dermatology Unit, University of Siena, 53100 Siena, Italy
[13]These authors contributed equally to this work
*Correspondence: gunnar.houge@helse-bergen.no
https://doi.org/10.1016/j.ajhg.2018.10.013.

Figure 1. Features of Individual 1, with the p.Leu610Pro DDR2 Variant
(A–C) Panels A–C show facial features, including a long philtrum, a short nose, a thin upper vermilion, midface retrusion, and narrow nostrils.
(D) Panel D shows mild cutaneous acquired syndactyly of fingers 3 and 4 and flexion contractures.
(E) Panel E shows corneal vascularization at age 54 years and development of complete corneal conjunctivalization and symblepharon formation.

conjunctivalization of the cornea and a reduction of her visual acuity to hand motion only. Her left eye has normal vision, but examination showed limbal stem-cell deficiency (LSCD), a superior corneal vascular pannus, reduction of the central corneal thickness to 419 μm, and endothelial-cell dysfunction with disruption of healthy hexagonal morphology (Figures 2A–2C). Fundoscopy showed normal retinal findings. Her facial features include a mild narrowing of the nasal bridge, mild lower-midface retrusion, and mild epicanthal folds. The lengths of her palpebral fissures are normal. She was diagnosed with hypothyroidism in her 20s. She has generalized thin skin and erythema.The hyperkeratosis of follicular orifices of her arms, neck, and chest resembles keratosis pilaris. Radiographs of the hands showed relatively normal phalanges with contractures. Radiographs of the feet showed small, hypodense distal phalanges and deformed middle phalanges, and in the 3-5th toe severe lateral angulation of the DIP joints could be seen (Figure 2H). She had enlarged frontal sinuses on skull films and no apparent osteolysis.

Her eldest daughter (individual 4) had a normal birth and health history in early childhood. She developed contractures of her fourth fingers at 4–5 years of age; these contractures were associated with painless, non-erythematous swelling of the involved joints. Her PIP contractures were ~90 degrees on the right fourth finger, but less severe on the left third finger. On her palms, she had associated scar-like thickening overlying the flexor tendons of the fourth digits (Figures 2K and 2L). She had a right cholesteatoma removed at age 4; this recurred and was removed again at age 8. On evaluation at age 8.5, she had a faint papular erythematous rash on her arms, face, neck, and chest; a 3 mm bluish papule with a punctate eschar on her right upper arm; and a soft, slightly bluish 1.5–2.5 cm mass on the sole of her left foot. Although her vision was normal, she had a superior corneal vascular pannus and reduced central corneal thickness (right eye

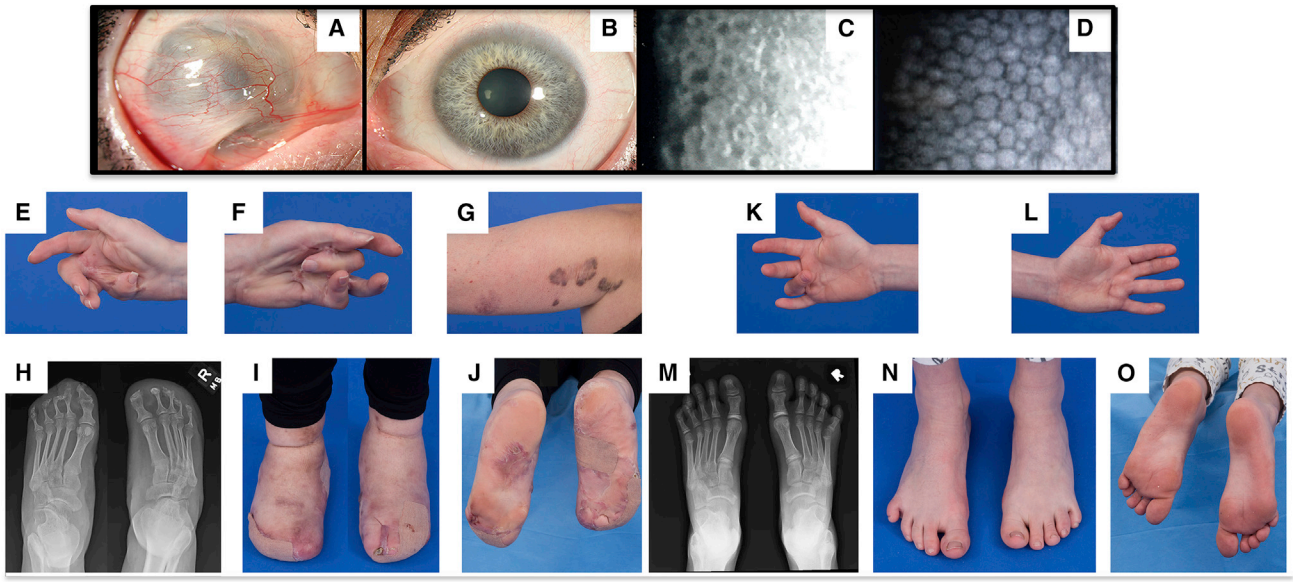

Figure 2. Features of Individuals 3 and 4
Individual 3 (A–J) is the index patient of this family, and individual 4 (K–O) is her 8-year-old daughter. Both have the p.Tyr740Cys *DDR2* variant.
(A and B) Slit-lamp microscopy images of the mother's anterior segment. There was complete conjunctivalization of the right cornea with symblepharon formation (A) and superior vascular pannus in the left eye (B).
(C) A specular microscopy image of the cornea of individual 3 (C). The image shows disruption of the healthy hexagonal endothelial morphology.
(D) A normal image is shown for comparison.
(E and F) Extreme flexion contractures of the mother's hands, as well as scarring and adhesions of the flexor surfaces of the digits and palm.
(G) A few of the annular plaques with features that are similar to those of keloids, though they have an atypical maroon-brown pigmentation. The more distal, lighter-pigmented lesion had been excised, after which it recurred and was treated with intralesional corticosteroids.
(H–J) Feet and radiographs featuring acro-osteolysis, lateral deviation of the digits, and extreme connective-tissue overgrowth leading to subsequent fusion of the toes.
(K–O) Images of the 8-year-old daughter show a 90-degree flexion contracture of the right fourth finger (K), scar-like lesions of the palm, mild contraction of the left fourth finger, and asubtle, scar-like lesion in the palm proximal to that digit (L). The radiograph shows an absence of major osteolysis in the feet, whichappeared largely normal aside from a deviated, deformed distal phalanx of the left fourth toe.

491 μm, left eye 484 μm), but normal endothelial cell morphology on specular microscopy. She has a long face with midface retrusion, a narrow nose, short palpebral fissures, epicanthal folds, and thin ear cartilage. Her skin is thin and somewhat lax, similar to her mother's, although her feet appear relatively normal.

The youngest child (individual 5) is a male with an unremarkable birth and health history, except for noticeable enlargement of several PIP finger joints and mild flexion contractures of several DIP finger joints. On evaluation at age 3, he had mild follicular hyperkeratosis, and an eye examination showed a prominent superior corneal vascular pannus. His facial features are essentially the same as those of his sister. The proband's third and healthy child, her brother, and both of her parents reportedly have none of the features described above. All individuals have apparently normal intelligence.

The sixth affected individual (individual 6) is a 35-year-old female who presented with a complex combination of congenital and acquired symptoms. She was born to healthy, unrelated parents with an unremarkable family history, apart from the presence of polycystic kidney disease in her father and paternal uncle. She presented with pyloric stenosis and facial dysmorphism in infancy. Psychomotor development was normal, but she suffered from recurrent ear infections that led to conductive hearing loss during childhood. In addition, she also has polycystic kidney disease. Her arms had angiodermatofibromas (benign and superficial fibrous histiocytoma), and her scalp had lichenoid skin lesions. Furthermore, she has hypothyroidism and mild mitral valve insufficiency, and during adolescence a susceptibility to bruising was noted. She has had surgical corrections of dental crowding and malpositioned teeth. At age 18 years, spontaneous pneumothorax was diagnosed. At age 22 years, she underwent sigmoid resection as a result of chronic diverticulitis and developed stenotic scarring as a later complication. At age 31years she had peritonitis after surgery associated with an ovarian abscess. Wound healing was delayed, and she developed a thick, protruding scar that in some areas was keloid-like. During treatment of her abdominal illness, she sustained an ischemic stroke, and she developed cysts in the liver. She has hypermobile joints, flat feet, contractures, and generalized joint enlargements of

Table 1. Overview of Phenotypic Features

	Individual 1	Individual 2	Individual 3	Individual 4	Individual 5	Individual 6
Described by	Warburg et al.[1]	Cinotti et al.[2]	this paper	this paper	this paper	this paper
Age	57 years	58 years	31 years	8 years	3 years	35 years
Familial status	singleton individual	singleton individual	index mother	child of individual 3	child of individual 3	singleton individual
DDR2 variant	p.Leu610Pro	p.Tyr740Cys	p.Tyr740Cys	p.Tyr740Cys	p.Tyr740Cys	p.Leu610Pro
Narrow palpebral fissures	+	+	–	+	NR	+
Corneal vascularization	+++	+++	++	+	+	NR
Reduced vision	+++	+++	++	–	NR	NR
Thin nose ± small alae nasi	+	+	+	+	+	+
Long face	+	–	+	+	+	NR
High palate	+	NR	–	–	–	+
Abnormal teeth	+	+	–	–	–	+
Posteriorly rotated ears	+	+	+	–	–	NR
Thin ear cartilage	NR	NR	+	+	NR	NR
Conductive hearing loss	+	–	–	NR	NR	+
Cholesteatoma	+	NR	NR	+	NR	NR
Skin with little subcutaneous tissue	+	NR	+	+	NR	+
Keloid-like plaques	+	+	+	–	–	+
Follicular hyperkeratosis	NR	NR	+	–	+	+
Contractures	++	+++	++	+	+	+
Joint swellings	NR	NR	+	+	+	+
Acro-osteolysis	+	+	+	–	–	+
Palmar fibrotic bands / cutaneous fusions	NR	+	+	+	–	–
Loss of toenails / toes	+	+	+	–	–	+
Pneumothorax	+	–	–	–	–	+
Mitral valve insufficiency	NR	+	–	–	–	+
Hypothyroidism	NR	NR	+	–	–	+
Intestinal problems	+	NR	–	–	–	++

Abbreviations are as follows: + = present, with degree of presence indicated when appropriate; – = absent; and NR = not reported.

the fingers. Chronic ulcerations on her toes eventually led to the loss of all toes and a significant portion of forefoot tissue. She has surgical wound management on a regular basis. At her latest clinical examination (at age 35), she presented with apparently normal cognition, tall stature (~95th percentile), reduced subcutaneous body fat, enlarged and low-set-ears, widely spaced eyes, bilateral epicanthus, bilateral blepharophimosis, a thin nose with small alae nasi, and a high palate. She is able to walk unsupported but suffers from limitations due to chronic ulcerations on her feet.

Clinical testing for genomic copy-number aberrations and a connective-tissue gene panel of individuals 1 and 2 were normal (data not shown). Research exome sequencing, using both dominant and recessive models, was undertaken as described in the Supplemental Methods. We made a list of all variants shared by these unrelated individuals, then removed all variants previously classified as benign in our diagnostic pipeline, as well as all variants present in dbSNP build 137. Only four heterozygous missense variants in two genes remained. Two variants were in *MUC4* [MIM: 158372] in non-conserved nucleotides and amino acids, and both were predicted to be benign by the *in silico* tools provided by Alamut (Interactive Biosoftware). Two variants were in *DDR2* [MIM: 191311]; these variants affected conserved nucleotides and amino acids, and both were predicted to be damaging by the following *in silico* prediction programs: PolyPhen2, MutationTester, SIFT, and LRT. Individual 1 was heterozygous for *DDR2* (GenBank: NM_001014796.1) c.1829T>C (p.Leu610Pro), and individual 2 was heterozygous for *DDR2* c.2219A>G (p.Tyr740Cys). In programs provided through Alamut,

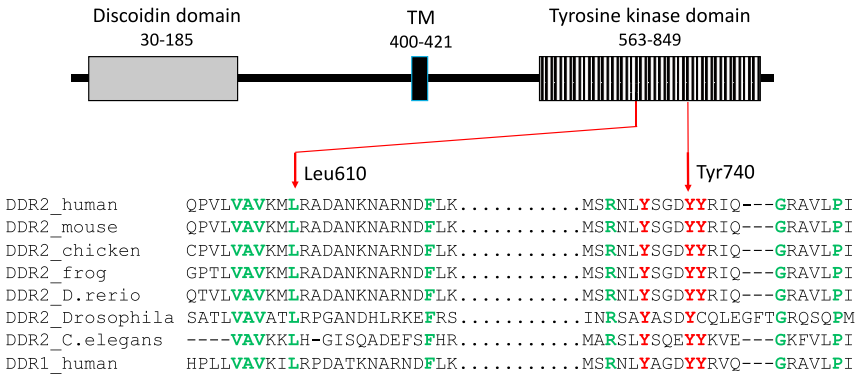

Figure 3. DDR2 Structure and Amino Acid Conservation
Above, the DDR2 structure is sketched with variant positions indicated. Below, the degree of amino acid conservation is indicated by a comparison to organisms ranging from *C. elegans* to humans. The paralog DDR1 is also included for comparison. Red Y's are tyrosines known to be phosphorylated. Green amino acids are conserved. TM = transmembrane domain.

neither of the variants were predicted to affect splicing. In addition, the variants had CADD scores of 30 for p.Leu610Pro and 31 for p.Tyr740Cys, also decreasing the likelihood that this was a chance finding (see Supplemental Methods for details). *DDR2* is relatively intolerant to loss-of-function variants (Exac database pLI score of 0.99) and more tolerant to missense variation (Exac database *Z* score of 2.09). Neither of the *DDR2* variants found were present in the gnomAD database, nor were any other missense changes to either the Leu610 or Tyr740 codons. Both missense changes affect conserved amino acids located in the DDR2 tyrosine kinase domain, as can be seen from the cross-species comparison made in Figure 3. The same amino acids are also conserved in DDR1 [MIM: 600408]. Subsequently, we found that individual 3 had the same p.Tyr740Cys variant previously found in individual 2 and that individual 6 had the same p.Leu610Pro variant previously found in individual 1. The variant found in individual 3 was proven to be *de novo* after parental testing (Figure S3). In the other individuals, samples from both parents were not available (Figures S1, S2, and S4). The two affected children of individual 3 (individuals 4 and 5) had inherited the p.Tyr740Cys variant (Figure S3). The variants were verified by Sanger sequencing (Figures S1–S3). We conclude that the identification of two unique and recurrent missense variants, p.Leu610Pro and p.Tyr740Cys, affecting conserved DDR2 amino acids, in four families with a similar clinical phenotype (one proven *de novo* occurrence) confirms the pathogenicity of these variants.

The discoidin domain receptors, DDR1 and DDR2, are receptor tyrosine kinases (RTKs) that are stimulated by collagen in the extracellular matrix (ECM). Unlike most other RTKs, they form ligand-independent stable dimers that are non-covalently linked.[3] This ECM activation induces receptor phosphorylation with slow kinetics, i.e., a slow and prolonged response, unlike the quicker responses of most other RTKs. DDRs regulate cell proliferation, differentiation, migration, and survival and control extracellular matrix homeostasis and remodeling. Dysregulated DDR function has been associated with fibrosis, arthritis, and cancer.[3,4] *DDR2* is predominantly expressed in fibroblasts, chondrocytes, osteoblasts, and other connective-tissue cells of mesenchymal origin.[5]

Both the p.Leu610Pro and the p.Tyr740Cys substitutions are located in the kinase domain of the DDR2 receptor. To study the consequences of these substitutions, we first examined DDR2 autophosphorylation. All results were reproduced in at least two independent experiments. Control fibroblasts and fibroblasts from individuals 1 and 3, heterozygous for the p.Leu610Pro and the p.Tyr740Cys substitutions, respectively, were cultured in Dulbecco's modified Eagle's medium (DMEM)—high glucose (Lonza) supplemented with 10% fetal calf serum, penicillin, streptomycin, and glutamine. When the cells were 80%–90% confluent, fresh medium was added, and the cells were harvested the following day. The total phosphorylated DDR2 was measured with a DuoSet IC Phospho-DDR2 kit (#DYC6170, R&D Systems) according to the manufacturer's recommendations (see Supplemental Methods). More phosphorylated DDR2 was observed in the fibroblasts from affected individuals than in those of controls, indicating that the variants were activating and caused autophosphorylation of the receptor (Figures 4A and 4B).

DDR2 has 14 tyrosine residues: four located in the extracellular juxtamembrane region, and the rest located in the kinase domain of the receptor.[6] Tyr740 is thought to play a critical role for DDR2 autoinhibition and site-directed Tyr740Phe mutagenesis caused *in vitro* DDR2 autophosphorylation and thereby mimicked the effect of high levels of SRC.[7] Because the p.Tyr740Cys variant alters this tyrosine residue, phosphorylation at this site was further examined. For immunoblot analyses, cells were starved of serum overnight before being harvested, separated on a high-resolution gel system, transferred to nitrocellulose membranes, and incubated overnight at 4°C with antibodies against phospho-Tyr740-DDR2 (#MAB25382) and DDR2 (#MAB2538) (R&D Systems, detailed description in Supplemental Methods). Anti-rabbit IgG (#7074) and anti-mouse IgG (#7076) (Cell Signaling Technology) were used as secondary antibodies. As a control for equal loading, the membranes were blocked again, incubated overnight with a GAPDH primary antibody (#G99545, Sigma-Aldrich), and visualized as described above. HEK293 cells transiently transfected with a human *DDR2* expression vector were used as a positive control (see Supplemental Methods). After use of an antibody against

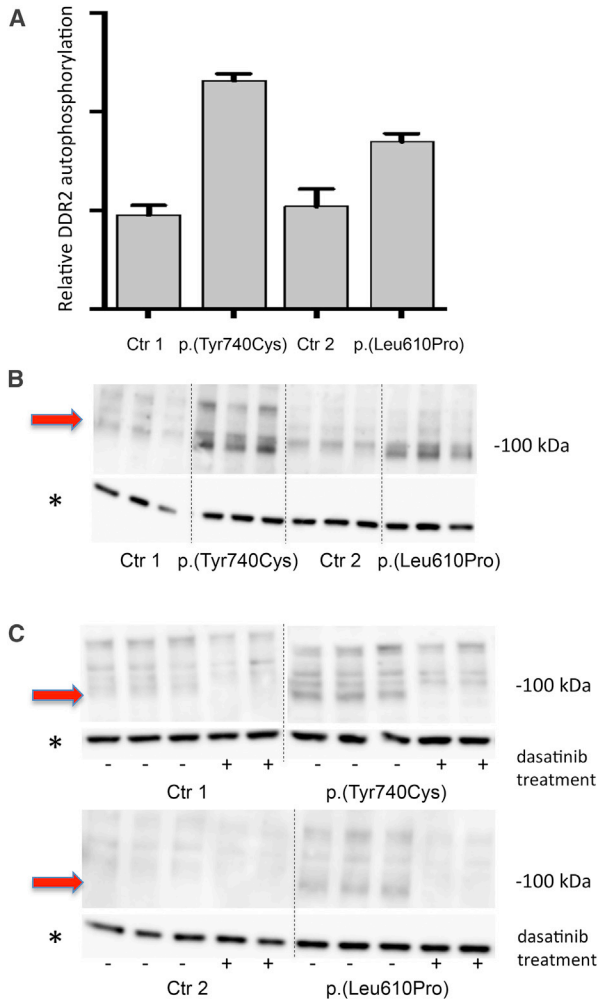

Figure 4. Autophosphorylation of DDR2 and Effect of Dasatinib Treatment

(A and B) ELISA (A) and immunoblot (B) results show that DDR2 phosphorylation is greater in fibroblasts with the p.Tyr740Cys or p.Leu610Pro substitutions than in control fibroblasts (Ctr 1 and Ctr 2). For ELISA (A), cells were harvested, and total phosphorylated DDR2 was measured with the DuoSet IC Phospho-DDR2 kit. For immunoblot analysis (B), cells that had been serum starved overnight were harvested and examined. The antibody used targeted phospho-Tyr740-DDR2. The band representing phospho-DDR2 is marked with a red arrow.

(C) The result of treatment with 0.1 μM dasatinib (+) in control fibroblasts (left lanes), fibroblasts from individual 3 (top right lanes), and fibroblasts from individual 1 (bottom right lanes). In fibroblasts with the p.Leu610Pro and p.Tyr740Cys substitution, the band representing phospho-DDR2 (marked with a red arrow) disappeared after dasatinib treatment. All experiments were reproduced in at least two independent experiments, and representative results are shown.

Error bars illustrate the standard deviation of replicated experiments.

non-phosphorylated DDR2, no DDR2 was detected in fibroblasts from affected individuals or controls (Figure S5). In contrast, the antibody against Tyr740-phosphorylated DDR2 left a clear band of expected size in fibroblasts harboring the p.Leu610Pro and p.Tyr740Cys substitutions, but not in controls (Figure 4B and Figure S6). Increased phosphorylation of Tyr740 in cells heterozygous for the p.Tyr740Cys variant suggested that autophosphorylation of the wild-type protein partner of a DDR2 dimer took place in these cells or that this antibody also binds to DDR2 if phosphorylated at nearby tyrosine residues, e.g., Tyr736 and Tyr741 (Figure 3). It is likely that both variants cause ligand-independent kinase activation, as has been described for other RTKs.[8]

The DDRs can interact with multiple proteins and also modulate signaling pathways initiated by other matrix receptors, cytokines,growth factors, and transmembrane receptors in a context- and cell-type-dependent manner.[3,4] We therefore evaluated the consequences of DDR2 activation on potential downstream growth-stimulatory pathways and STAT1. The latter is an important modifier in the overgrowth and tissue wasting seen in individuals with *PDGFRB* [MIM: 173410] gain-of-function variants.[9] The following proteins were assessed with appropriate antibodies, all obtained from Cell Signaling Technology at recommended dilutions (see Supplemental Methods for details): phospho-Tyr542-PTPN11(SHP-2), phospho-Tyr580-PTPN11(SHP-2), PTPN11(SHP-2), phospho-Ser473-AKT, AKT, phospho-Thr202/Tyr204-MAPK3(ERK1), MAPK3(ERK1), phospho-Tyr416-SRC, Tyr416-SRC, phospho-Tyr527-SRC, Tyr527-SRC, SRC, and phospho-Tyr70-STAT1. We did not detect increased phosphorylation of any of these proteins (Figures S7–S21). This suggests that the consequence of DDR2 activation in Warburg-Cinotti syndrome (MIM: 618175) is targeted to a group of proteins with little signal-transduction crosstalk with well-known growth-stimulatory pathways, such as the RAS/ERK and PI3K/AKT pathways.

Our finding that activating *DDR2* variants are a cause of this disease suggested that the ABL inhibitor dasatinib, a leukemia drug that also inhibits DDR2, could be used for treatment of affected individuals.[10,11] To examine the effect of dasatinib on p.Leu610Pro- and p.Tyr740Cys-induced autophosphorylation, we cultured fibroblasts from affected individuals and controls as described above. When the cells were 80%–90% confluent, the medium was replaced with serum-free DMEM. After 16 hours, cells were either left untreated or treated with 0.05 or 0.1μM dasatinib (#S1021, Selleckchem); they were then harvested after 6 hours as described above. Immunoblot analysis determined the presence of phospho-Tyr740-DDR2. At both concentrations, dasatinib abolished the observed autophosphorylation of DDR2 (Figure4C and Figures S22 and S23), providing *invitro* support for experimental treatment of affected individuals. Penttinen syndrome, associated with activating mutations in *PDGFRB,* and Warburg-Cinottisyndrome have many similarities, such as lipodystrophy, subcutaneous-tissue wasting and accompanying hypertrophic lesions, and marked acro-osteolysis.[12] Of note, PDGF-targeted therapy has been effective in three reported individuals with germline activating *PDGFRB* mutations.[13,14]

DDR2 is an important regulator of bone growth and resorption, both as a promoter of osteoblastogenesis and

as an inhibitor of osteoclastogenesis.[15,16] DDR2 has been suggested as a therapeutic target for osteoporosis.[16] In addition, DDR2-collagen interaction stimulates the secretion of lysyl oxidase, which cross-links collagen fibers in the ECM.[3,17] Why activating mutations in *DDR2* might be associated with osteolysis in the individuals described here remains to be elucidated. However, bi-allelic loss-of-function variants in *DDR2* cause spondylometaepiphyseal dysplasia accompanied by short limbs and abnormal (premature) calcifications (SMED-SL [MIM: 271665]).[18,19] This developmental disorder is associated with decreased bone formation but not increased bone destruction (or osteolysis). No skin or eye changes have been reported.[18–20] The individuals described in this report had normal or tall stature and normal limb lengths, indicating normal developmental bone growth. They also had an acquired arthropathy with osteolysis that was associated with flexion contractures. Premature calcifications (as seen in SMED-SL) were not observed in any of the individuals with Warburg-Cinotti syndrome. Thus, the phenotype of the individuals reported here with gain-of-function DDR2 variants was distinct from that seen in SMED-SL, which is associated with loss-of-function DDR2 variants.

The individuals described here experienced corneal vascularization in early adult life. DDR2 is able to both drive and prevent angiogenesis under different conditions.[21–23] The primary effect seems to be angiogenesis stimulation, but a rebound effect or overcompensation can counterbalance this.[22] In several of the individuals, limbal stem-cell deficiency (LSCD) was detected at an early age. The corneal epithelium undergoes constant shedding and regeneration to maintain optic clarity. The surrounding limbus forms a barrier to protect the cornea from neovascularization. In LSCD this barrier is disrupted, and the corneal epithelium might be replaced with conjunctival cells, similar to what we observed in these individuals. Although symptoms of LSCD often include signs of inflammation (redness and irritation), corneal neovascularization might also develop in the absence of such signs. One example is in aniridia caused by haploinsufficiency of *PAX6*.[24,25]

The individuals described here had multiple skin problems, including thin skin, chronic ulcers, and a tendency to form keloid-like lesions. In mice, the highest levels of phosphorylated DDR2 were found in the lungs, ovaries, and skin.[26] DDR2 is thought to be both a marker and key regulator of the epithelial-mesenchymal transition.[22] DDR2 signaling is important for wound healing through multiple mechanisms: chemotactic migration to the wounded area, proliferation, synthesis and remodeling of the wound matrix by collagen cross-linking, and finally, fibroblast-mediated contraction of the healing wound. Inhibition of DDR2 activity has been postulated as a therapeutic option to improve wound healing and reduce keloid formation,[27] which is supported by our data.

Several of the keloid-like lesions seen in these individuals were pigmented. It is of potential relevance that genetic variants in *DDR1* [MIM: 600408] have been associated with vitiligo, and DDR1 activation is involved when melanocytes are attached to collagen-IV fibers.[28] Because DDR1 and DDR2 are paralogous receptors, we hypothesize that activated DDR2 has a role in the migration or function of melanocytes.

In conclusion, we have identified the cause of a fibrotic syndrome that is inherited in an autosomal-dominant pattern. This syndrome is characterized by corneal vascularization, acro-osteolysis, contractures, thin skin, keloid-like plaques, and ulcerations, particularly of the toes and feet. We suggest it should be designated Warburg-Cinotti syndrome, after the authors of the first two clinical reports. In addition, we have identified a family and another singleton individual with the same condition. All affected individuals had activating variants in DDR2, either p.Leu610Pro or p.Tyr740Cys. We show that dasatinib inhibited the ligand-independent DDR2 autophosphorylation induced by both variants *in vitro*, suggesting an approach for treatment.

Supplemental Data

Supplemental Data include 23 figures, Supplemental Methods, and one table and can be found with this article online at https://doi.org/10.1016/j.ajhg.2018.10.013.

Acknowledgments

We thank Unni Larsen for technical assistance and Raoul C.M. Hennekam and Karen Brøndum-Nielsen for professional assistance. The work was supported by grants from the Western Norway Regional Health Authority (911977 and 912161 to C.B.), the Dr. Jon S. Larsens Foundation (to C.B.), and the Olav Raagholt and Gerd Meidel Raagholt Foundation for Research (to C.B.). L.G.B., J.J.J., and J.C.S. were supported by the Intramural Research Program of the National Human Genome Research Institute, grants HG200328 12 and HG200388 04. The NIH Intramural Sequencing Center performed exome sequencing on the family identified at the NIH (individuals 3–5).

Declaration of Interests

L.G.B. is an uncompensated advisor to the Illumina Corporation, receives royalties from Genentech, and in-kind research support from ArQule. The other authors declare no competing interests.

Received: July 3, 2018
Accepted: October 15, 2018
Published: November 15, 2018

Web Resources

ClinVar, https://www.ncbi.nlm.nih.gov/clinvar/
Exac Browser, http://exac.broadinstitute.org/
GnomAD Browser, http://gnomad.broadinstitute.org/
Online Mendelian Inheritance in Man, http://www.omim.org/

References

1. Warburg, M., Ullman, S., Jensen, H., Pedersen, H., Kobayashi, T., Russell, B., Tranebjaerg, L., Richard, G., and Brøndum-Nielsen, K.

(2006). Blepharophimosis, corneal vascularization, deafness, and acroosteolysis: A "new" syndrome? Am. J. Med. Genet. A. *140*, 2709–2713.
2. Cinotti, E., Ferrero, G., Paparo, F., Papadia, M., Faravelli, F., Rongioletti, F., Traverso, C., and Di Maria, E. (2013). Arthropathy, osteolysis, keloids, relapsing conjunctival pannus and gingival overgrowth: A variant of polyfibromatosis? Am. J. Med. Genet. A. *161A*, 1214–1220.
3. Leitinger, B. (2014). Discoidin domain receptor functions in physiological and pathological conditions. Int. Rev. Cell Mol. Biol. *310*, 39–87.
4. Borza, C.M., and Pozzi, A. (2014). Discoidin domain receptors in disease. Matrix Biol. *34*, 185–192.
5. Alves, F., Vogel, W., Mossie, K., Millauer, B., Höfler, H., and Ullrich, A. (1995). Distinct structural characteristics of discoidin I subfamily receptor tyrosine kinases and complementary expression in human cancer. Oncogene *10*, 609–618.
6. Valiathan, R.R., Marco, M., Leitinger, B., Kleer, C.G., and Fridman, R. (2012). Discoidin domain receptor tyrosine kinases: New players in cancer progression. Cancer Metastasis Rev. *31*, 295–321.
7. Yang, K., Kim, J.H., Kim, H.J., Park, I.S., Kim, I.Y., and Yang, B.S. (2005). Tyrosine 740 phosphorylation of discoidin domain receptor 2 by Src stimulates intramolecular autophosphorylation and Shc signaling complex formation. J. Biol. Chem. *280*, 39058–39066.
8. Chen, H., Marsiglia, W.M., Cho, M.K., Huang, Z., Deng, J., Blais, S.P., Gai, W., Bhattacharya, S., Neubert, T.A., Traaseth, N.J., and Mohammadi, M. (2017). Elucidation of a four-site allosteric network in fibroblast growth factor receptor tyrosine kinases. eLife *6*.
9. He, C., Medley, S.C., Kim, J., Sun, C., Kwon, H.R., Sakashita, H., Pincu, Y., Yao, L., Eppard, D., Dai, B., et al. (2017). STAT1 modulates tissue wasting or overgrowth downstream from PDGFRβ. Genes Dev. *31*, 1666–1678.
10. Terai, H., Tan, L., Beauchamp, E.M., Hatcher, J.M., Liu, Q., Meyerson, M., Gray, N.S., and Hammerman, P.S. (2015). Characterization of DDR2 inhibitors for the treatment of DDR2 mutated nonsmall cell lung cancer. ACS Chem. Biol. *10*, 2687–2696.
11. Liu, L., Hussain, M., Luo, J., Duan, A., Chen, C., Tu, Z., and Zhang, J. (2017). Synthesis and biological evaluation of novel dasatinib analogues as potent DDR1 and DDR2 kinase inhibitors. Chem. Biol. Drug Des. *89*, 420–427.
12. Johnston, J.J., Sanchez-Contreras, M.Y., Keppler-Noreuil, K.M., Sapp, J., Crenshaw, M., Finch, N.A., Cormier-Daire, V., Rademakers, R., Sybert, V.P., and Biesecker, L.G. (2015). A point mutation in PDGFRB causes autosomal-dominant penttinen syndrome. Am. J. Hum. Genet. *97*, 465–474.
13. Mudry, P., Slaby, O., Neradil, J., Soukalova, J., Melicharkova, K., Rohleder, O., Jezova, M., Seehofnerova, A., Michu, E., Veselska, R., and Sterba, J. (2017). Case report: Rapid and durable response to PDGFR targeted therapy in a child with refractory multiple infantile myofibromatosis and a heterozygous germline mutation of the PDGFRB gene. BMC Cancer *17*, 119.
14. Pond, D., Arts, F.A., Mendelsohn, N.J., Demoulin, J.B., Scharer, G., and Messinger, Y. (2018). A patient with germ-line gain-of-function PDGFRB p.N666H mutation and marked clinical response to imatinib. Genet. Med. *20*, 142–150.
15. Lin, K.L., Chou, C.H., Hsieh, S.C., Hwa, S.Y., Lee, M.T., and Wang, F.F. (2010). Transcriptional upregulation of DDR2 by ATF4 facilitates osteoblastic differentiation through p38 MAPK-mediated Runx2 activation. J. Bone Miner. Res. *25*, 2489–2503.
16. Zhang, Y., Su, J., Wu, S., Teng, Y., Yin, Z., Guo, Y., Li, J., Li, K., Yao, L., and Li, X. (2015). DDR2 (discoidin domain receptor 2) suppresses osteoclastogenesis and is a potential therapeutic target in osteoporosis. Sci. Signal. *8*, ra31.
17. Khosravi, R., Sodek, K.L., Faibish, M., and Trackman, P.C. (2014). Collagen advanced glycation inhibits its discoidin domain receptor 2 (DDR2)-mediated induction of lysyl oxidase in osteoblasts. Bone *58*, 33–41.
18. Bargal, R., Cormier-Daire, V., Ben-Neriah, Z., Le Merrer, M., Sosna, J., Melki, J., Zangen, D.H., Smithson, S.F., Borochowitz, Z., Belostotsky, R., and Raas-Rothschild, A. (2009). Mutations in DDR2 gene cause SMED with short limbs and abnormal calcifications. Am. J. Hum. Genet. *84*, 80–84.
19. Ali, B.R., Xu, H., Akawi, N.A., John, A., Karuvantevida, N.S., Langer, R., Al-Gazali, L., and Leitinger, B. (2010). Trafficking defects and loss of ligand binding are the underlying causes of all reported DDR2 missense mutations found in SMED-SL patients. Hum. Mol. Genet. *19*, 2239–2250.
20. Ge, C., Wang, Z., Zhao, G., Li, B., Liao, J., Sun, H., and Franceschi, R.T. (2016). Discoidin receptor 2 controls bone formation and marrow adipogenesis. J. Bone Miner. Res. *31*, 2193–2203.
21. Zhang, S., Bu, X., Zhao, H., Yu, J., Wang, Y., Li, D., Zhu, C., Zhu, T., Ren, T., Liu, X., et al. (2014). A host deficiency of discoidin domain receptor 2 (DDR2) inhibits both tumour angiogenesis and metastasis. J. Pathol. *232*, 436–448.
22. Zhao, H., Bian, H., Bu, X., Zhang, S., Zhang, P., Yu, J., Lai, X., Li, D., Zhu, C., Yao, L., and Su, J. (2016). Targeting of discoidin domain receptor 2 (DDR2) prevents myofibroblast activation and neovessel formation during pulmonary fibrosis. Mol. Ther. *24*, 1734–1744.
23. Zhu, T., Zhu, J., Bu, X., Zhao, H., Zhang, S., Chang, Y., Li, R., Yao, L., Wang, Y., and Su, J. (2015). The anti-angiogenic role of discoidin domain receptor 2 (DDR2) in laser-induced choroidal neovascularization. J. Mol. Med. (Berl.) *93*, 187–198.
24. Lim, P., Fuchsluger, T.A., and Jurkunas, U.V. (2009). Limbal stem cell deficiency and corneal neovascularization. Semin. Ophthalmol. *24*, 139–148.
25. Gonzalez, G., Sasamoto, Y., Ksander, B.R., Frank, M.H., and Frank, N.Y. (2018). Limbal stem cells: identity, developmental origin, and therapeutic potential. Wiley Interdiscip. Rev. Dev. Biol. *7*.
26. Labrador, J.P., Azcoitia, V., Tuckermann, J., Lin, C., Olaso, E., Mañes, S., Brückner, K., Goergen, J.L., Lemke, G., Yancopoulos, G., et al. (2001). The collagen receptor DDR2 regulates proliferation and its elimination leads to dwarfism. EMBO Rep. *2*, 446–452.
27. Márquez, J., and Olaso, E. (2014). Role of discoidin domain receptor 2 in wound healing. Histol. Histopathol. *29*, 1355–1364.
28. Ricard, A.S., Pain, C., Daubos, A., Ezzedine, K., Lamrissi-Garcia, I., Bibeyran, A., Guyonnet-Dupérat, V., Taieb, A., and Cario-André, M. (2012). Study of CCN3 (NOV) and DDR1 in normal melanocytes and vitiligo skin. Exp. Dermatol. *21*, 411–416.

The American Journal of Human Genetics, Volume *103*

Supplemental Data

Recurrent, Activating Variants in the Receptor Tyrosine Kinase *DDR2* Cause Warburg-Cinotti Syndrome

Linda Xu, Hanne Jensen, Jennifer J. Johnston, Emilio Di Maria, Katja Kloth, Ileana Cristea, Julie C. Sapp, Thomas N. Darling, Laryssa A. Huryn, Lisbeth Tranebjærg, Elisa Cinotti, Christian Kubisch, Eyvind Rødahl, Ove Bruland, Leslie G. Biesecker, Gunnar Houge, and Cecilie Bredrup

Figure S1: Pedigree of individual 1

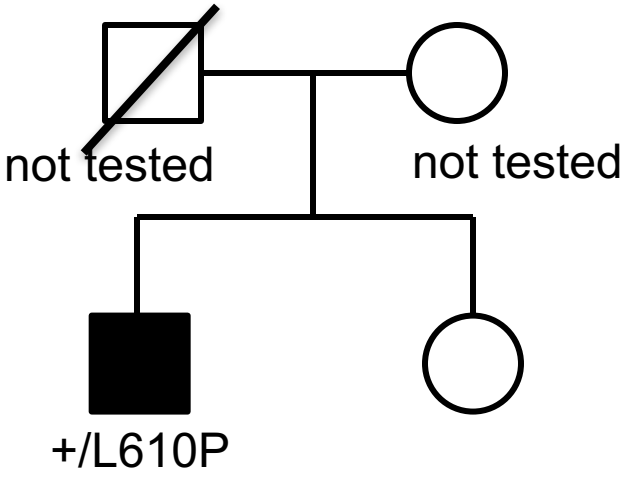

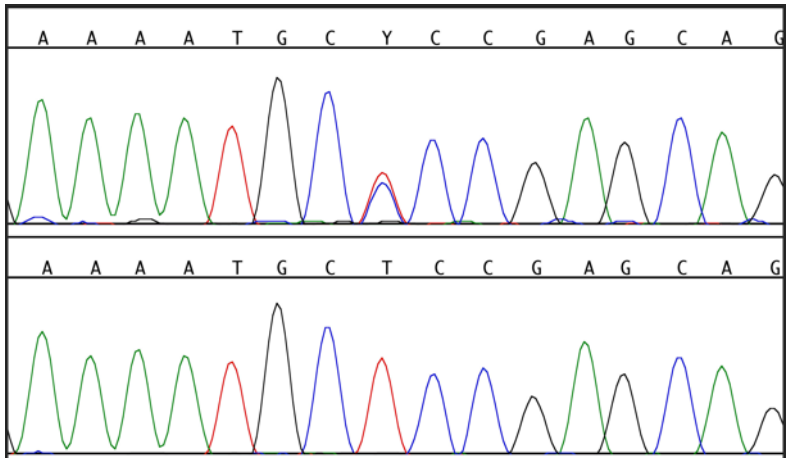

DDR2(NM_001014796) c.1829T>C, p.(Leu610Pro)

Control DNA sample

De novo occurrence of the mutation could not be proven as DNA from the father was not available.

Figure S2: Pedigree of individual 2

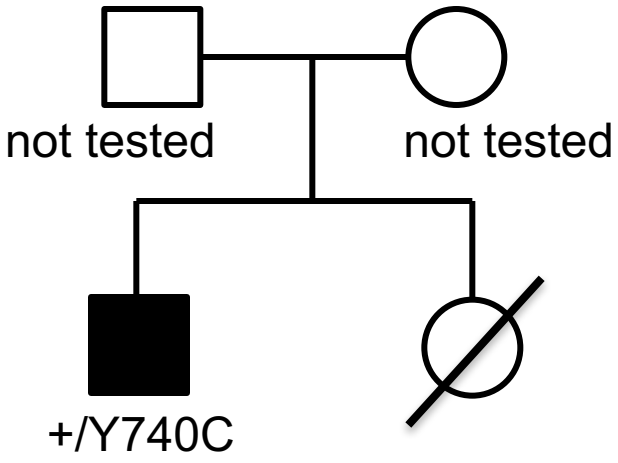

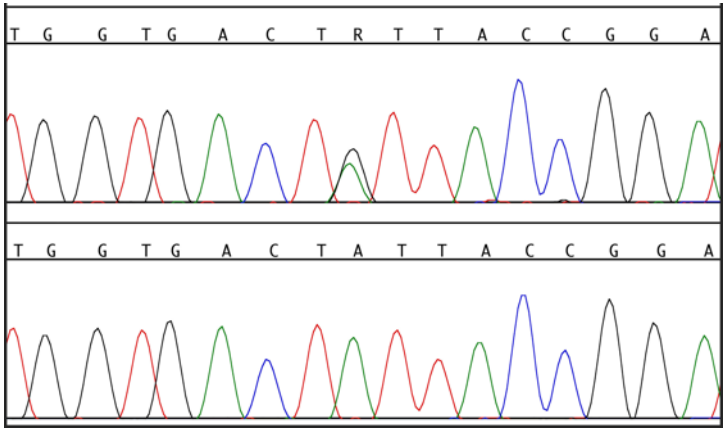

DDR2(NM_001014796) c.2219A>G, p.(Tyr740Cys)

Control DNA sample

De novo occurrence of the mutation could not be proven as DNA from the parents was not available.

Figure S3: Pedigree of individuals 3-5

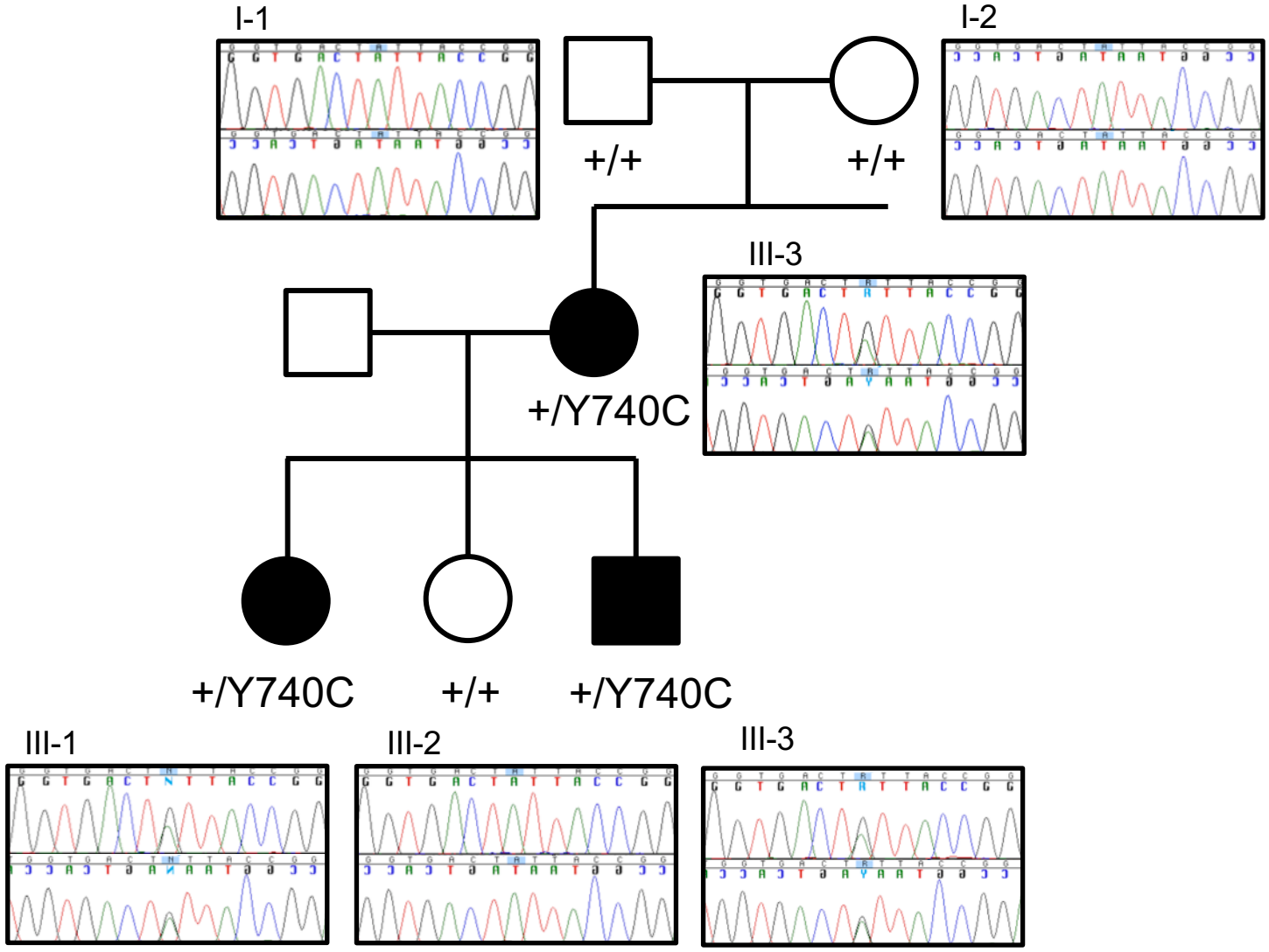

The mutation was proven *de novo* in II-2, and a biological relationship with II-1 and II-2 was verified. The electropherograms display the results of forward (top panels) and reverse (bottom panels) sequences.

Figure S4: Pedigree of individual 6

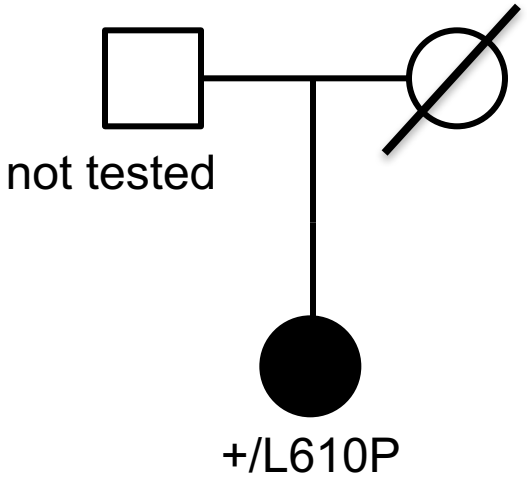

De novo occurrence of the mutation could not be proven as DNA from the parents was not examined.

Figure S5: DDR2 immunoblot results

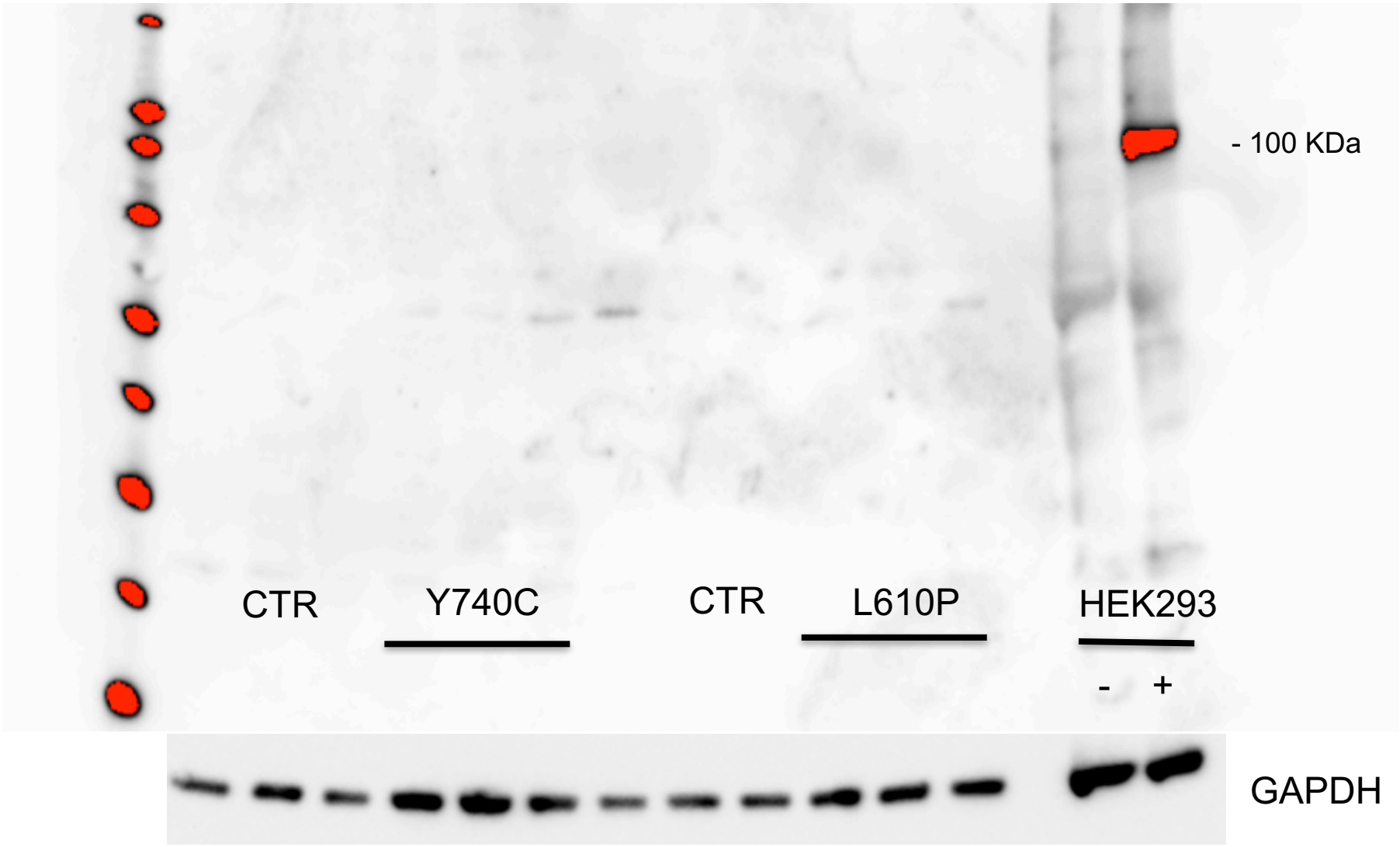

Immunoblot analysis of fibroblasts harboring the p.(Leu610Pro) and the p.(Tyr740Cys) substitutions. DDR2 was undetectable in these cells. HEK 293 cells untransfected (-) or transfected (+) with DDR2 was used as control. Results from 3 parallel experiments.

Figure S6: Phospho-DDR2 immunoblot results

A

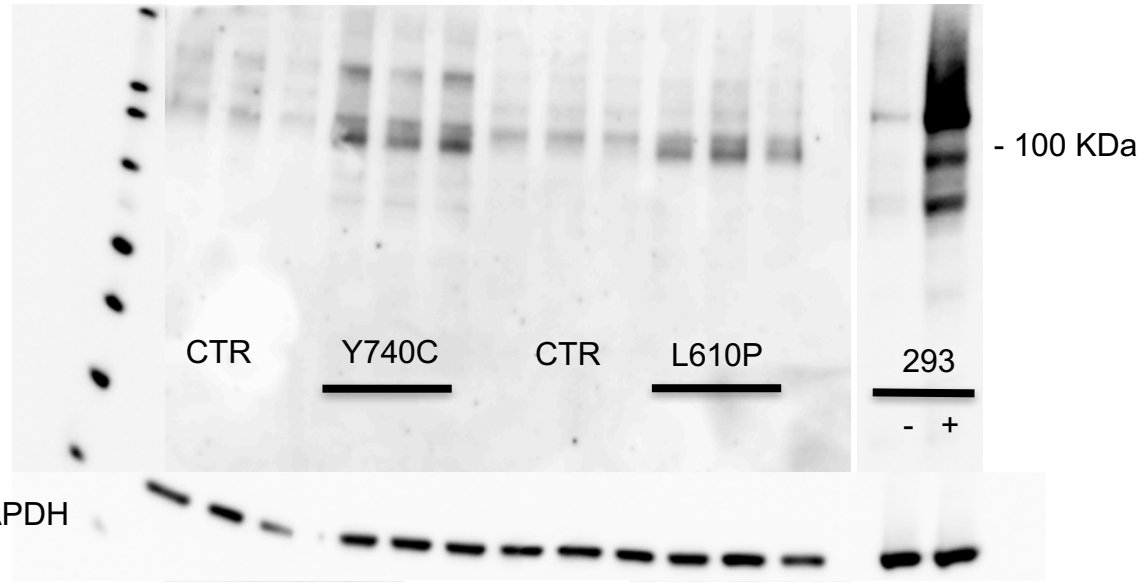

B

	P-DDR2	GAPDH	Corrected
CTR1a	1,00	1,00	1,00
CTR1b	2,18	1,02	2,14
CTR1c	1,70	0,45	3,74
Y740Ca	5,36	0,99	5,43
Y740Cb	7,18	1,15	6,21
Y740Cc	6,50	1,13	5,77
CTR2a	1,00	1,00	1,00
CTR2b	1,02	1,10	0,92
CTR2c	1,03	1,10	0,94
L610Pa	2,10	1,13	1,86
L610Pb	3,01	1,35	2,23
L610Pc	1,95	0,90	2,17

C

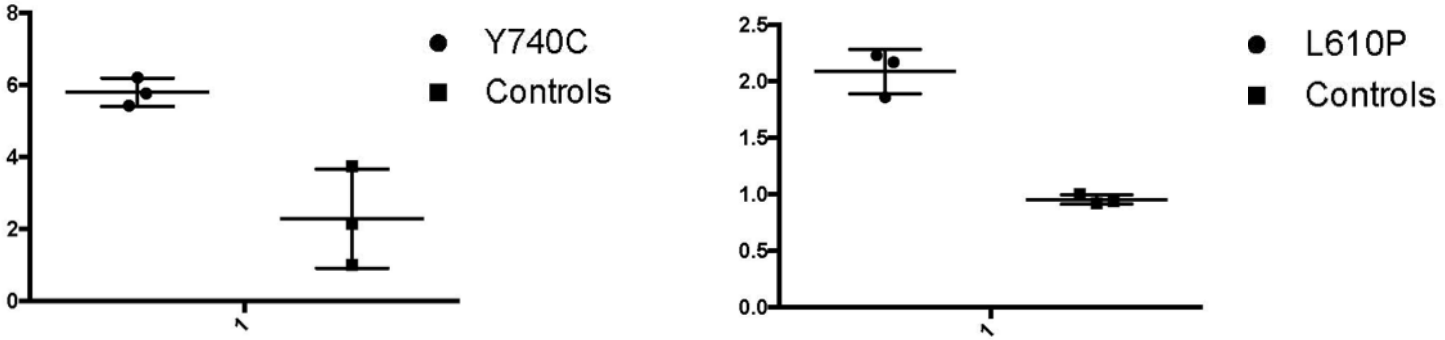

A: Immunoblot analysis of fibroblasts harboring the p.(Leu610Pro) and the p.(Tyr740Cys) substitutions. Increased levels of phospho-DDR2 (P-Tyr740) was detectable in patient fibroblast (Y740C and L610P). HEK 293 cells untransfected (-) or transfected (+) with DDR2 was used as control. Results from 3 parallel experiments.
B and C: results from relative quantifications. Measured values are approximately twice as high in fibroblasts from affected individuals. P=0.1 due to some variability in parallel experiments.

Figure S7: Phospho-Tyr542-PTPN11/SHP-2 immunoblot results

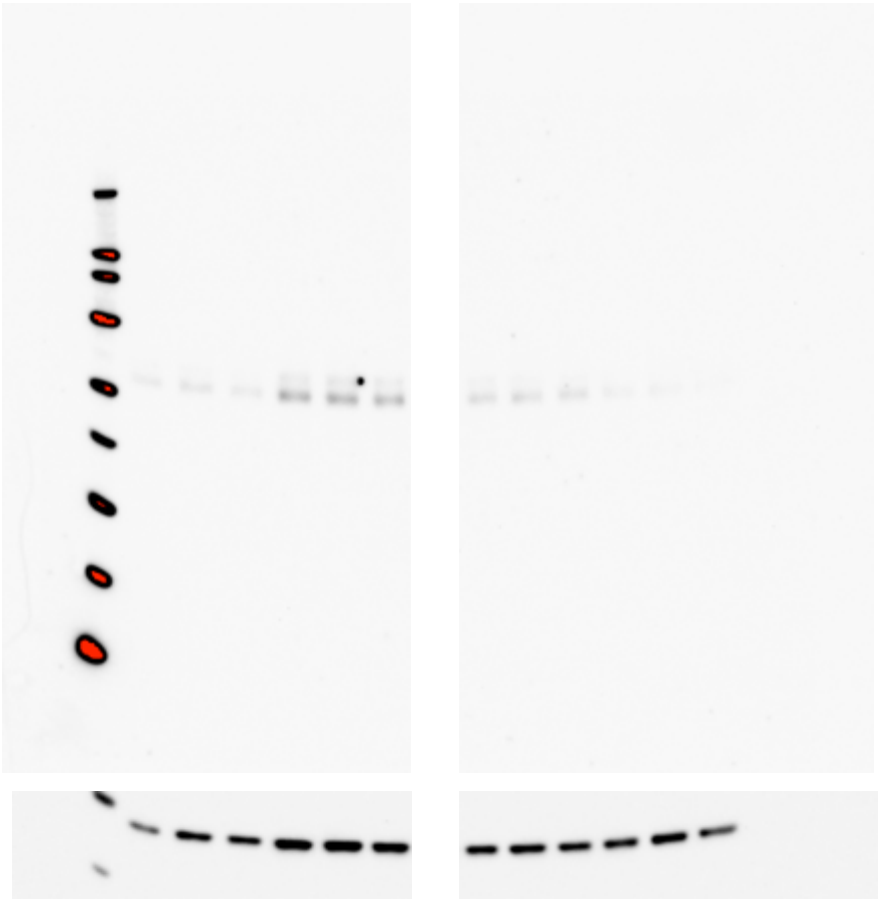

GAPDH

	P-Tyr542	GAPDH	Corrected
Ctr. A1	1,00	1,00	1,00
Ctr. A2	1,62	2,11	0,77
Ctr. A3	1,06	1,75	0,61
Y740C 1	7,01	3,54	1,98
Y740C 2	5,62	3,88	1,45
Y740C 3	4,74	3,06	1,55
L610P 1	2,62	1,98	1,32
L610P 2	2,25	2,39	0,94
L610 3	2,04	1,89	1,08
Ctr. B1	0,69	1,94	0,36
Ctr. B2	0,61	2,63	0,23
Ctr. B3	0,32	1,64	0,19

Immunoblot analysis of fibroblasts harboring the p.(Leu610Pro) and the p.(Tyr740Cys) substitutions. Slightly higher levels of phosphop-Tyr542-PTPN11 were found but this was not satistically significant. Results from 3 parallel experiments.

Figure S8: Phospho-Tyr580-PTPN11 immunoblot results

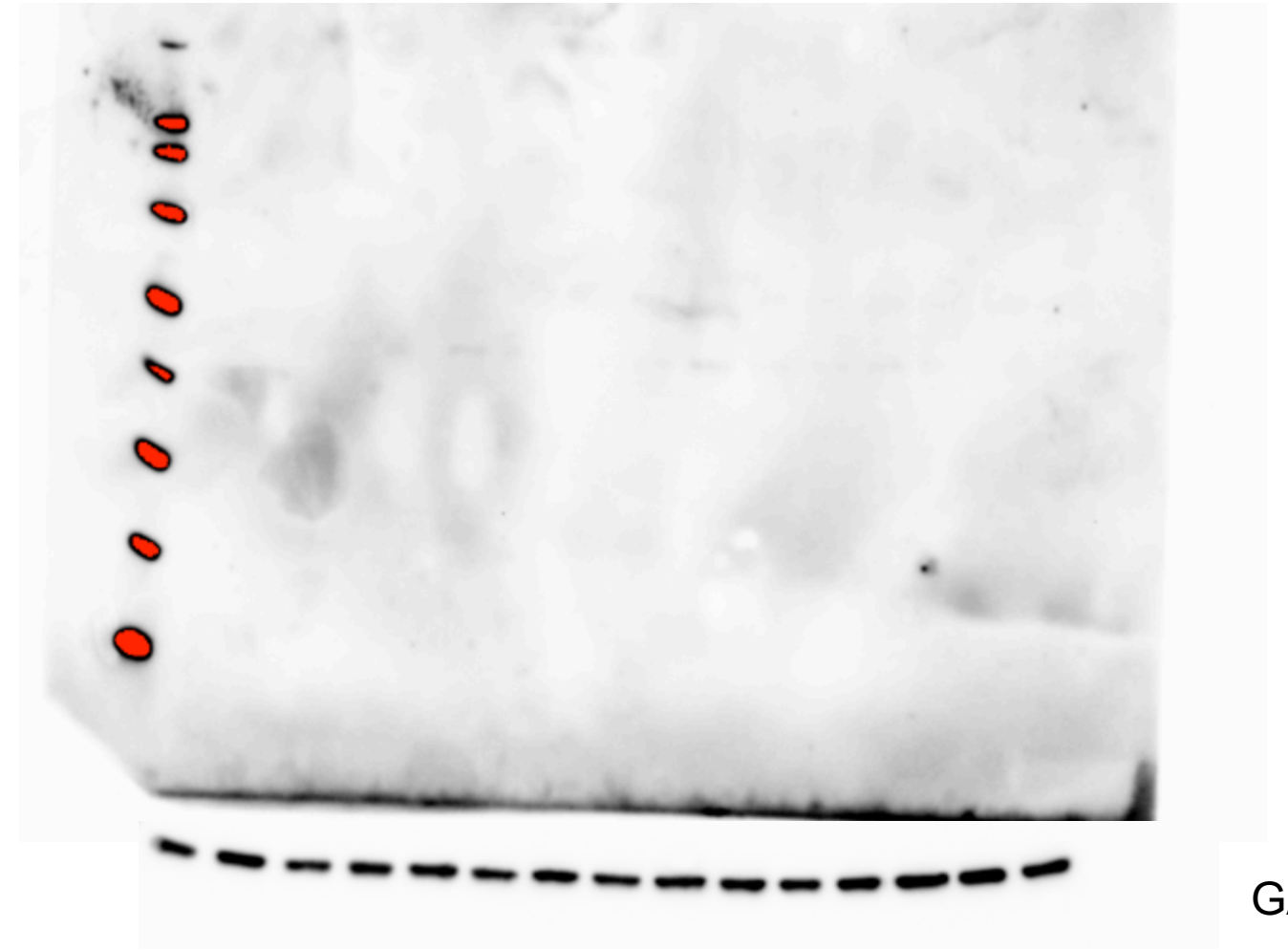

Immunoblot analysis of fibroblasts harboring the p.(Leu610Pro) and the p.(Tyr740Cys) substitutions. Phospho-Tyr580-PTPN11 was not detectable. Results from 3 parallel experiments.

Figure S9: PTPN11/SHP-2 immunoblot results

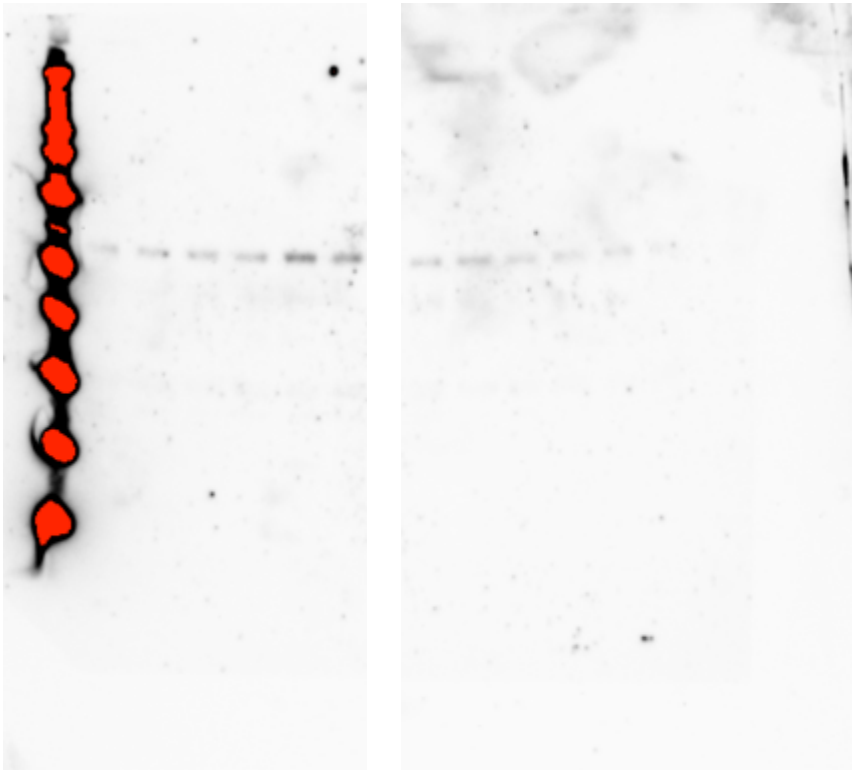

GAPDH

	PTPN11	GAPDH	Corrected
Ctr. A1	1,00	1,00	1,00
Ctr. A2	1,21	1,22	0,99
Ctr. A3	1,49	1,03	1,45
Y740C 1	1,58	1,64	0,97
Y740C 2	3,66	2,06	1,77
Y740C 3	3,75	1,62	2,32
L610P 1	1,21	1,19	1,02
L610P 2	1,72	1,33	1,29
L610 3	1,09	0,99	1,10
Ctr. B1	0,93	1,38	0,67
Ctr. B2	0,86	1,06	0,82
Ctr. B3	0,55	0,68	0,81

Immunoblot analysis of fibroblasts harboring the p.(Leu610Pro) and the p.(Tyr740Cys) substitutions. Slightly higher levels of PTPN11 were found but were not considered significant.
Results from 3 parallel experiments.

Figure S10: Phospho-AKT immunoblot results

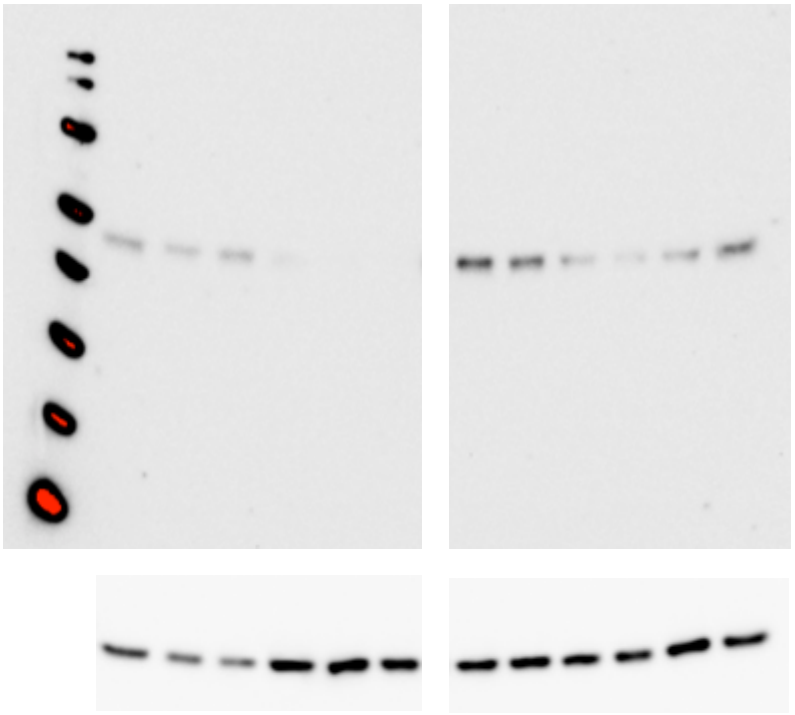

GAPDH

	P-AKT.	GAPDH.	Corrected
Ctr. A1	1,00	1,00	1,00
Ctr. A2	0,45	0,63	0,72
Ctr. A3	0,66	0,56	1,18
Y740C 1	0,17	1,83	0,09
Y740C 2	0,06	2,03	0,03
Y740C 3	0,07	1,44	0,05
L610P 1	2,17	1,44	1,51
L610P 2	1,61	1,58	1,02
L610 3	0,56	1,19	0,47
Ctr. B1	0,25	1,08	0,23
Ctr. B2	0,75	2,03	0,37
Ctr. B3	1,68	1,37	1,22

Immunoblot analysis of fibroblasts harboring the p.(Leu610Pro) and the p.(Tyr740Cys) substitutions. Slightly higher levels of phospho-AKT were found cells with the p.(Leu610Pro) substitution but this was not considered significant. Results from 3 parallel experiments.

Figure S11: AKT immunoblot results

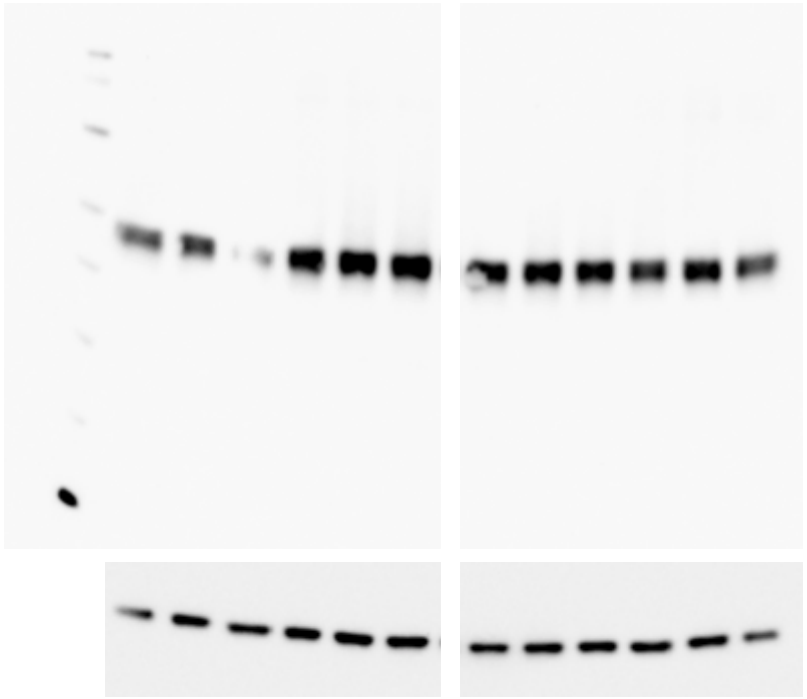

	AKT	GAPDH	Corrected
Ctr. A1	1,00	1,00	1,00
Ctr. A2	1,02	1,84	0,56
Ctr. A3	0,26	1,65	0,16
Y740C 1	1,67	2,11	0,79
Y740C 2	2,12	2,35	0,90
Y740C 3	2,31	2,50	0,92
L610P 1	1,46	1,69	0,86
L610P 2	1,73	1,92	0,90
L610 3	1,66	1,89	0,88
Ctr. B1	1,30	1,86	0,70
Ctr. B2	1,57	1,91	0,82
Ctr. B3	1,19	1,04	1,14

Immunoblot analysis of fibroblasts harboring the p.(Leu610Pro) and the p.(Tyr740Cys) substitutions. Similar levels of AKT were present. Results from 3 parallel experiments.

Figure S12: Phospho-MAPK3/ERK1 immunoblot results

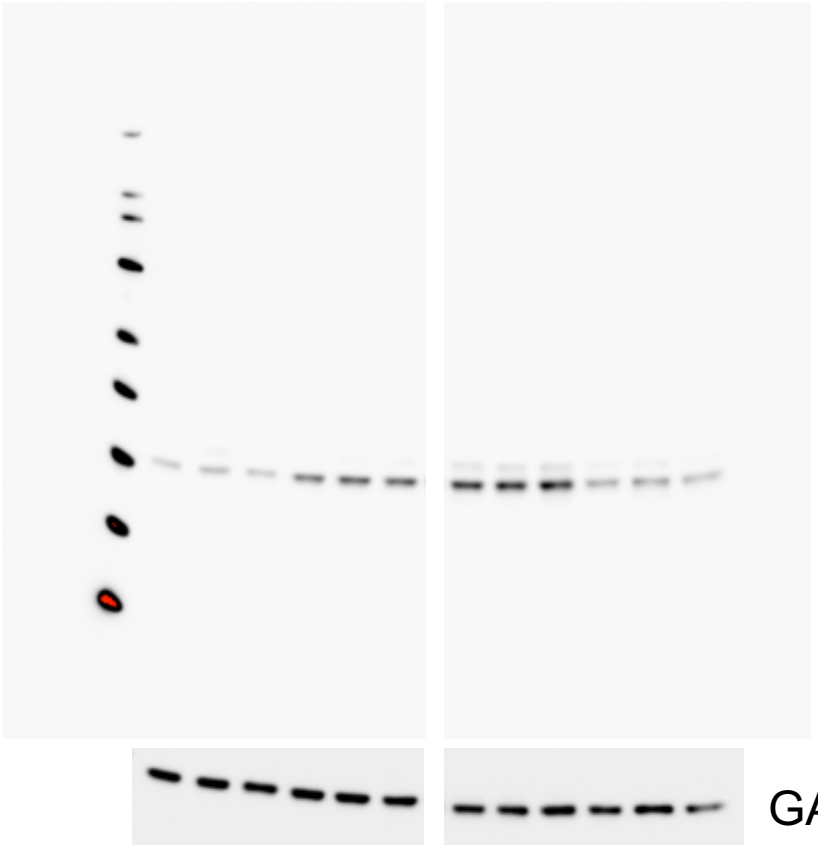

	P-ERK.	GAPDH	Corrected
Ctr. A1	1,00	1,00	1,00
Ctr. A2	1,28	1,00	1,28
Ctr. A3	1,01	0,86	1,17
Y740C 1	3,14	1,09	2,89
Y740C 2	3,94	1,05	3,74
Y740C 3	3,82	0,90	4,24
L610P 1	5,26	0,71	7,43
L610P 2	5,56	0,73	7,63
L610 3	6,23	0,90	6,93
Ctr. B1	2,10	0,67	3,12
Ctr. B2	2,57	0,92	2,79
Ctr. B3	1,78	0,50	3,53

Immunoblot analysis of fibroblasts harboring the p.(Leu610Pro) and the p.(Tyr740Cys) substitutions. Higher levels of phospho-MAPK3/ERK1 were found but were not reproduced in follow-up experiments as shown in Figure S14. Results from 3 parallel experiments.

Figure S13: MAPK3/ERK1 immunoblot results

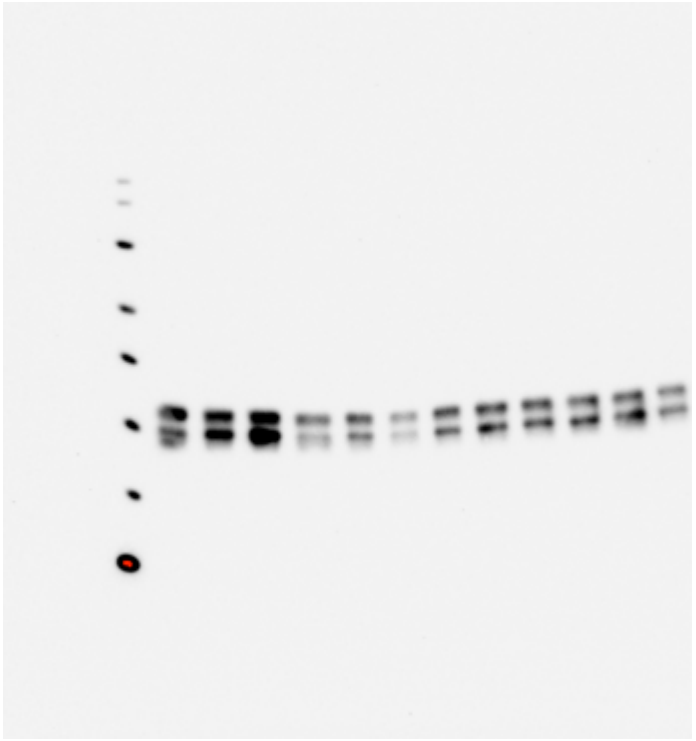

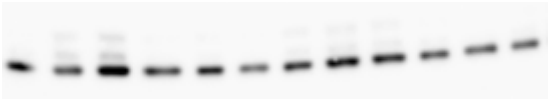

GAPDH

	ERK	GAPDH	Corrected
Ctr. A1	1,95	0,93	2,10
Ctr. A2	2,13	0,93	2,28
Ctr. A3	3,35	1,83	1,83
Y740C 1	1,00	1,00	1,00
Y740C 2	0,97	0,88	1,10
Y740C 3	0,44	0,64	0,69
L610P 1	1,02	0,86	1,18
L610P 2	1,43	1,24	1,15
L610 3	1,32	1,06	1,24
Ctr. B1	1,35	0,74	1,82
Ctr. B2	1,55	0,77	2,01
Ctr. B3	0,85	0,66	1,29

Immunoblot analysis of fibroblasts harboring the p.(Leu610Pro) and the p.(Tyr740Cys) substitutions. Similar levels of MAPK3/ERK1 was present. Results from 3 parallel experiments.

Figure S14: Phospho-MAPK3/ERK1 immunoblot results

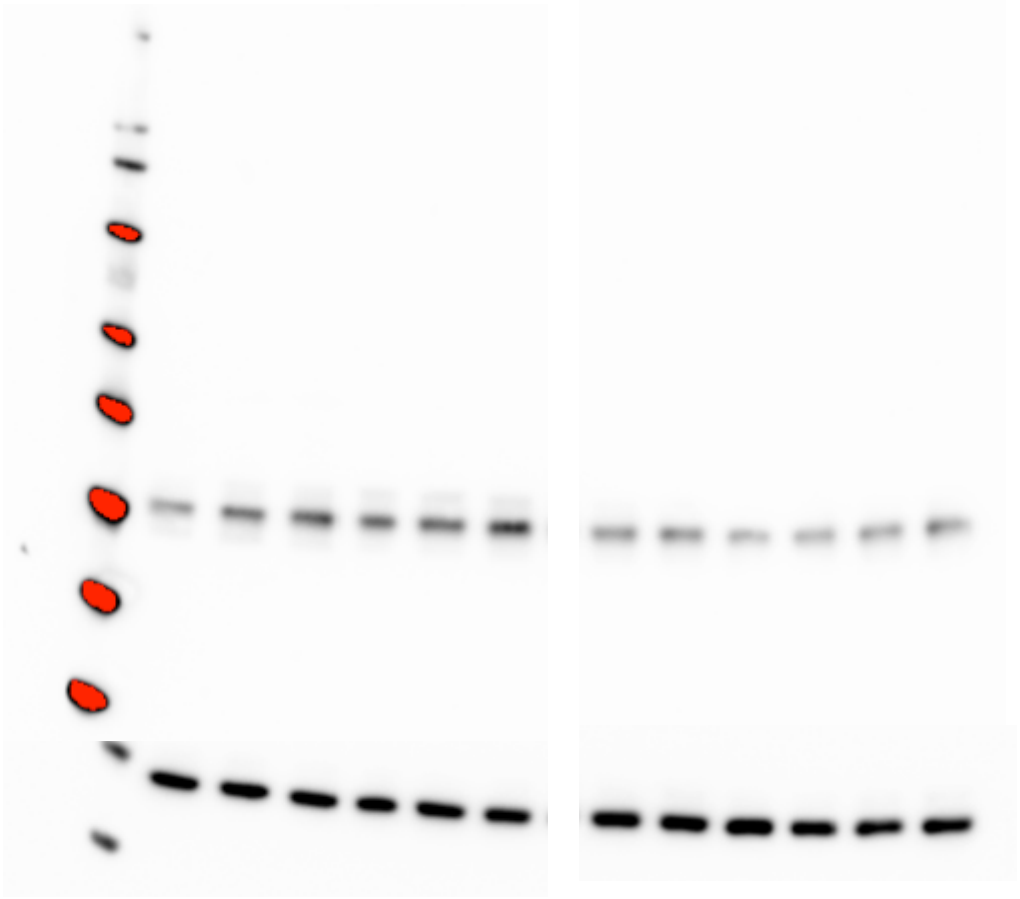

GAPDH

	P-ERK	GAPDH	Corrected
Ctr. C1	1,00	1,00	1,00
Ctr. C2	1,55	0,98	1,57
Ctr. C3	1,77	0,92	1,93
Y740C 1	1,45	0,80	1,80
Y740C 2	1,61	0,95	1,69
Y740C 3	2,16	0,85	2,54
L610P 1	1,16	1,06	1,10
L610P 2	1,15	1,07	1,07
L610 3	0,68	1,14	0,59
Ctr. D1	0,78	0,86	0,90
Ctr. D2	0,97	0,82	1,19
Ctr. D3	1,11	0,94	1,18

Immunoblot analysis of fibroblasts harboring the p.(Leu610Pro) and the p.(Tyr740Cys) substitutions. Due to the finding higher levels of phospho-MAPK3/ERK1 shown in Figure S12 this was reproduced. In this experiment slightly higher levels of phospho-ERK were found in cells with the p.(Tyr740Cys) substitution but were not considered significant. Results from 3 parallel experiments.

Figure S15: MAPK3/ERK1 immunoblot results

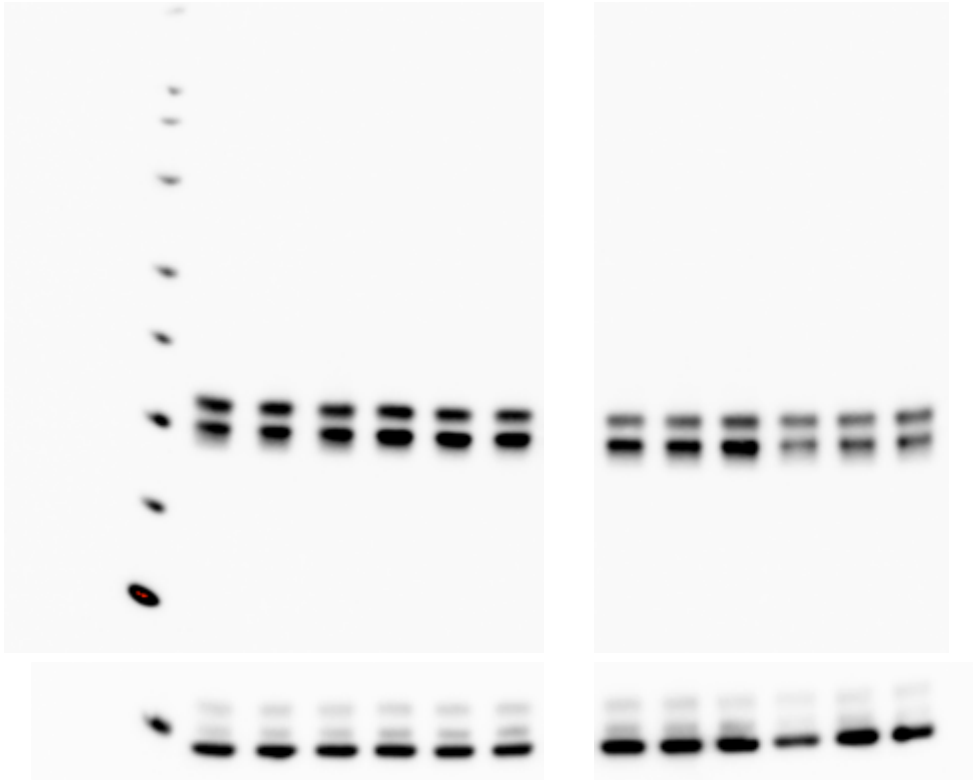

GAPDH

	GAPDH	ERK	Corrected
Ctr. C1	1,00	1,00	1,00
Ctr. C2	1,02	1,03	1,01
Ctr. C3	0,96	1,08	1,13
Y740C 1	1,04	1,31	1,26
Y740C 2	0,97	1,19	1,23
Y740C 3	0,93	1,13	1,21
L610P 1	1,45	0,89	0,61
L610P 2	1,45	0,93	0,64
L610 3	1,43	1,15	0,80
Ctr. D1	0,75	0,66	0,87
Ctr. D2	1,54	0,76	0,49
Ctr. D3	1,09	0,74	0,68

Immunoblot analysis of fibroblasts harboring the p.(Leu610Pro) and the p.(Tyr740Cys) substitutions. Similar levels of ERK was present. Results from 3 parallel experiments.

Figure S16: Phospho-Tyr416-SRC immunoblot results

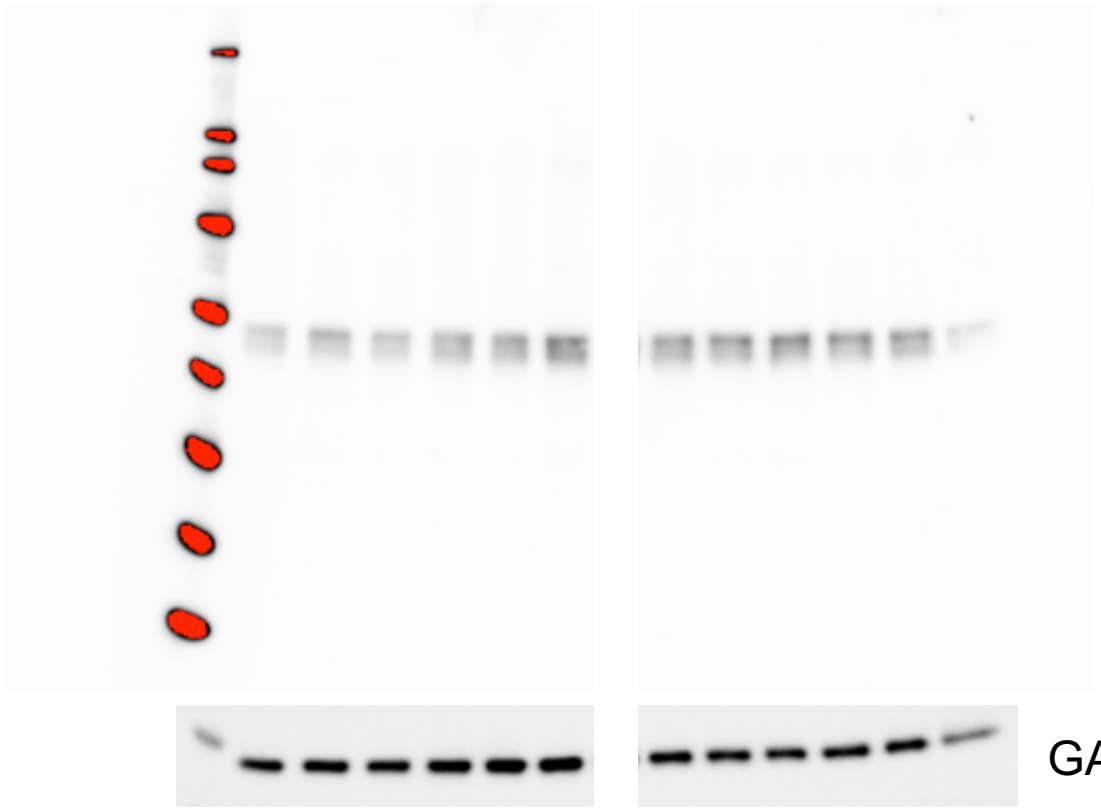

	P-SRC417	GAPDH	Corrected
Ctr. A1	1,00	1,00	1,00
Ctr. A2	1,40	1,22	1,15
Ctr. A3	1,10	1,05	1,05
Y740C 1	1,62	1,36	1,19
Y740C 2	1,64	1,51	1,09
Y740C 3	2,49	1,61	1,55
L610P 1	2,00	1,17	1,71
L610P 2	2,02	1,08	1,87
L610 3	2,10	0,95	2,21
Ctr. B1	1,92	1,10	1,75
Ctr. B2	1,75	1,02	1,72
Ctr. B3	0,45	0,61	0,74

Immunoblot analysis of fibroblasts harboring the p.(Leu610Pro) and the p.(Tyr740Cys) substitutions. Similar levels of phospho-Tyr416-SRC were present. Results from 3 parallel experiments.

Figure S17: Tyr416-SRC immunoblot results

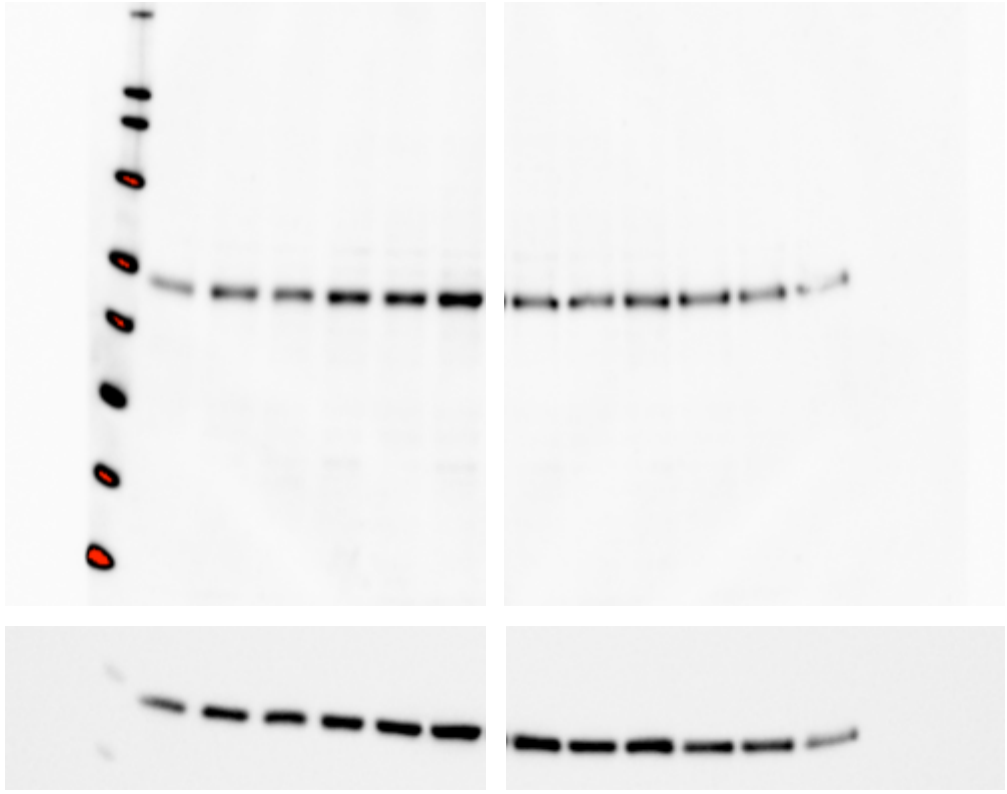

GAPDH

	SRC416	GAPDH	Corrected
Ctr. A1	1,00	1,00	1,00
Ctr. A2	1,73	1,55	1,11
Ctr. A3	1,49	1,41	1,06
Y740C 1	2,16	1,73	1,25
Y740C 2	2,17	1,98	1,10
Y740C 3	3,20	2,60	1,23
L610P 1	1,77	2,28	0,92
L610P 2	1,51	1,83	0,82
L610 3	1,94	2,04	0,95
Ctr. B1	1,76	1,49	1,18
Ctr. B2	1,40	1,41	0,99
Ctr. B3	0,68	0,81	0,84

Immunoblot analysis of fibroblasts harboring the p.(Leu610Pro) and the p.(Tyr740Cys) substitutions. Similar levels of Tyr416-SRC was present. Results from 3 parallel experiments.

Figure S18: Phospho-Tyr527-SRC immunoblot results

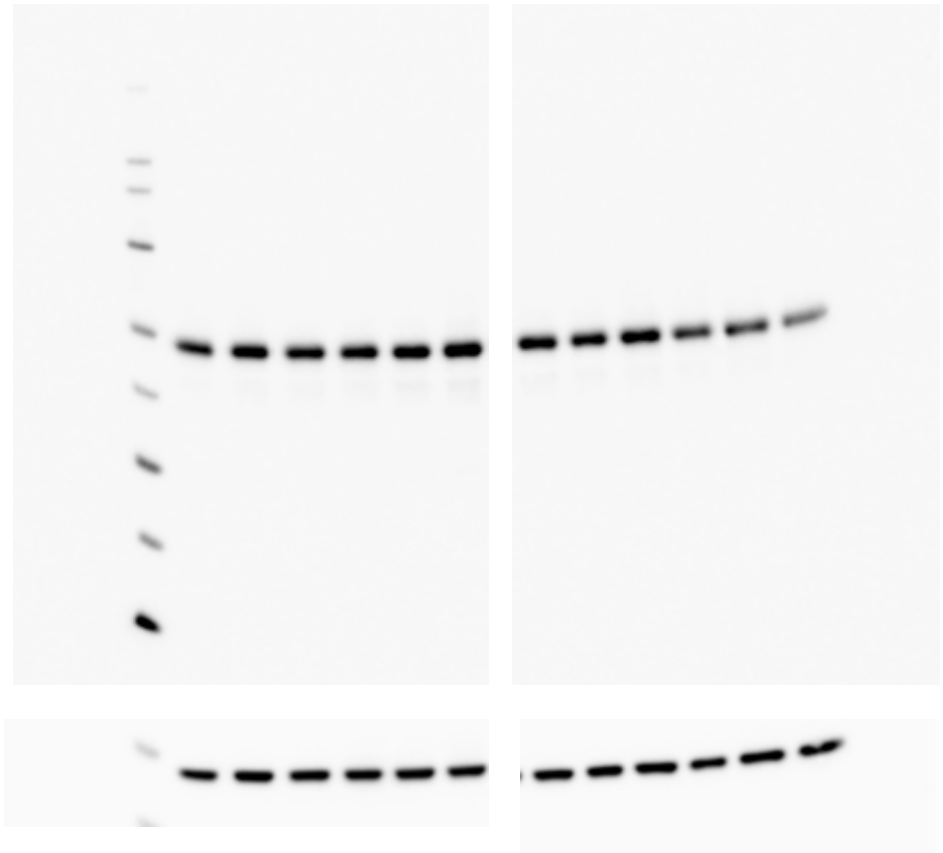

GAPDH

	P-SRC527	GAPDH	Corrected
Ctr. A1	1,00	1,00	1,00
Ctr. A2	1,33	1,32	1,01
Ctr. A3	1,23	1,25	0,99
Y740C 1	1,26	1,19	1,05
Y740C 2	1,42	1,24	1,14
Y740C 3	1,63	1,16	1,40
L610P 1	1,29	1,24	1,04
L610P 2	1,16	1,20	0,96
L610 3	1,43	1,37	1,05
Ctr. B1	0,98	1,03	0,95
Ctr. B2	1,07	1,41	0,76
Ctr. B3	0,76	1,24	0,61

Immunoblot analysis of fibroblasts harboring the p.(Leu610Pro) and the p.(Tyr740Cys) substitutions. Similar levels of phospho-Tyr527-SRC were present. Results from 3 parallel experiments.

Figure S19: Tyr527-SRC immunoblot results

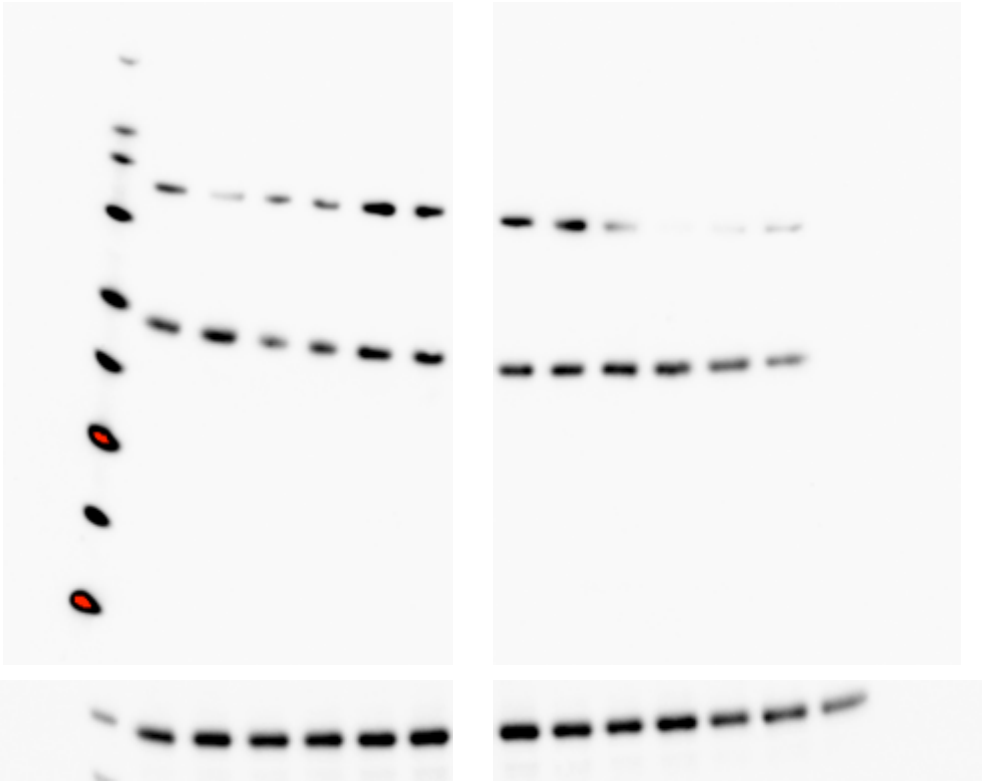

GAPDH

	SRC527	GAPDH	Corrected
Ctr. A1	1,00	1,00	1,00
Ctr. A2	1,38	0,94	1,47
Ctr. A3	0,55	0,50	1,10
Y740C 1	0,75	0,58	1,29
Y740C 2	1,37	0,73	1,89
Y740C 3	1,13	0,48	2,34
L610P 1	1,11	0,55	2,04
L610P 2	1,07	0,59	1,83
L610 3	1,21	0,65	1,85
Ctr. B1	1,16	0,62	1,88
Ctr. B2	1,01	0,77	1,31
Ctr. B3	0,47	0,63	0,75

Immunoblot analysis of fibroblasts harboring the p.(Leu610Pro) and the p.(Tyr740Cys) substitutions. Similar levels of Tyr527-SRC were present. Results from 3 parallel experiments.

Figure S20: SRC immunoblot results

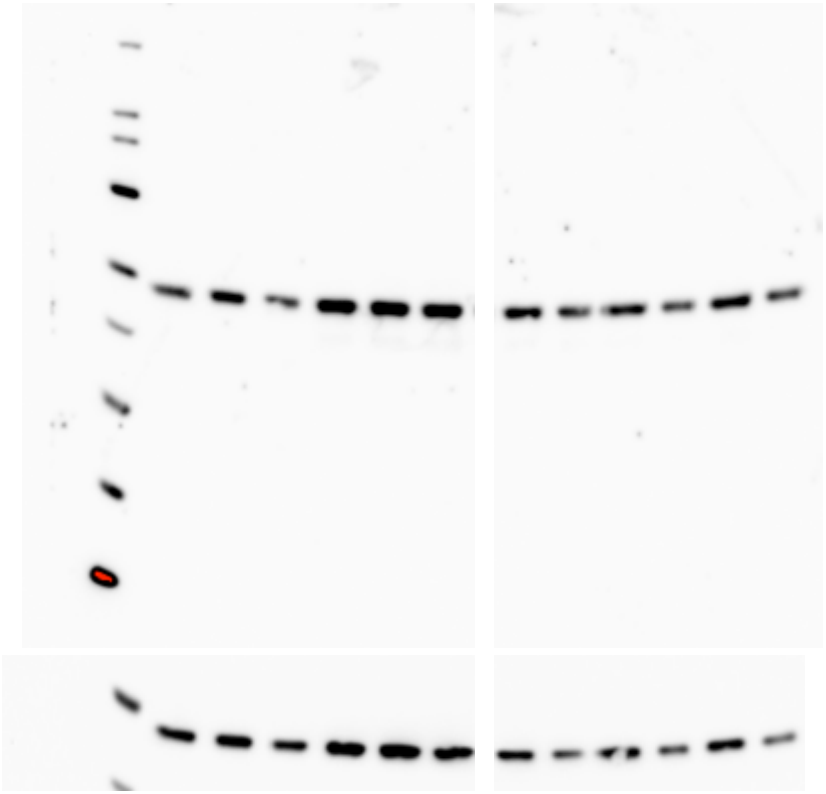

GAPDH

	Total SRC	GAPDH	Corrected
Ctr. A1	1,00	1,00	1,00
Ctr. A2	1,33	1,17	1,14
Ctr. A3	0,75	0,76	0,98
Y740C 1	2,24	1,70	1,32
Y740C 2	2,55	1,96	1,30
Y740C 3	2,39	1,39	1,72
L610P 1	1,39	0,83	1,67
L610P 2	0,93	0,47	1,97
L610 3	1,28	0,76	1,68
Ctr. B1	0,77	0,48	1,60
Ctr. B2	1,49	0,90	1,65
Ctr. B3	0,89	0,43	2,05

Immunoblot analysis of fibroblasts harboring the p.(Leu610Pro) and the p.(Tyr740Cys) substitutions. Similar levels of total SRC was present. Results from 3 parallel experiments.

Figure S21: Phospho-STAT1 immunoblot results

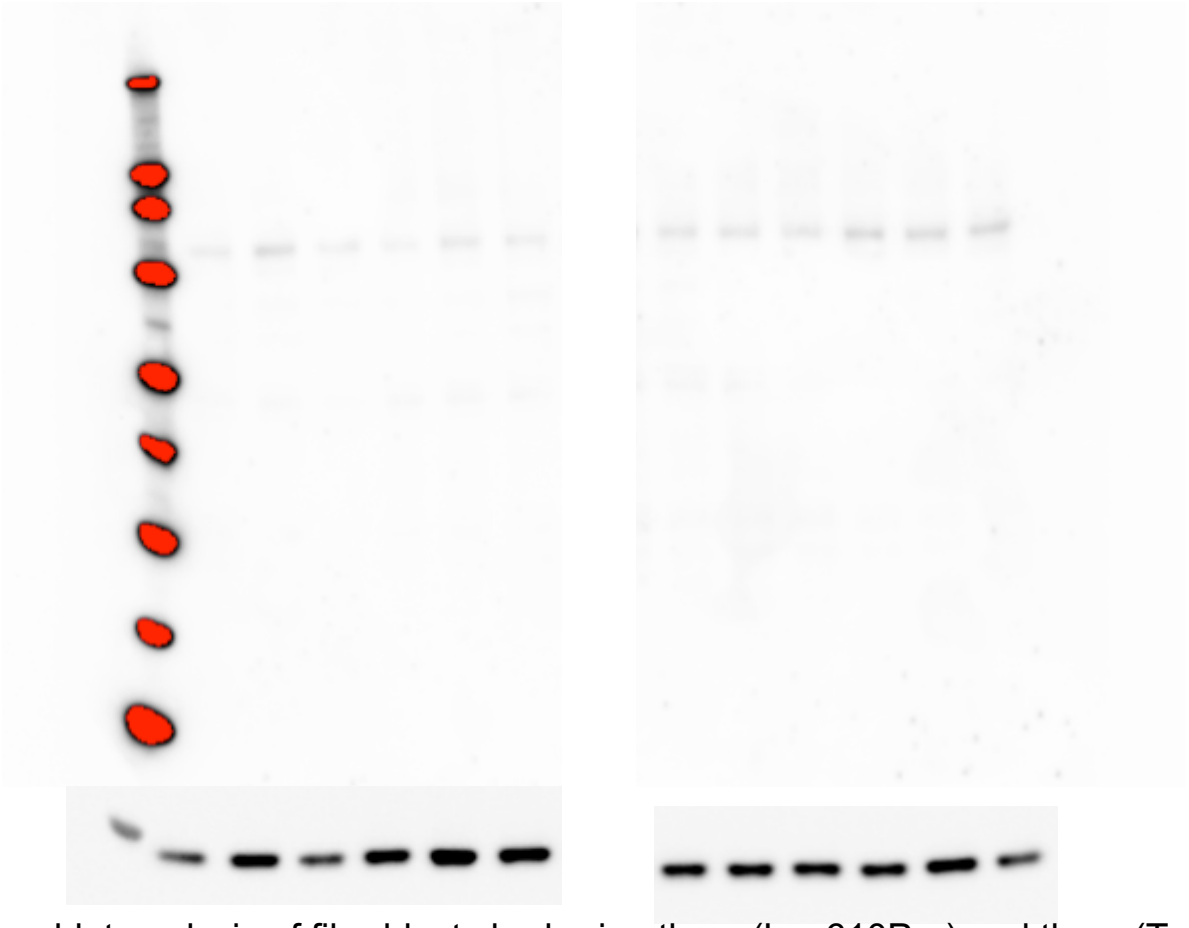

Immunoblot analysis of fibroblasts harboring the p.(Leu610Pro) and the p.(Tyr740Cys) substitutions. Similar levels of total Phospho-STAT1 was present. Bands were not measured due to low intensity. Results from 3 parallel experiments.

Figure S22: Phosho-DDR2 immunoblot results after dasatinib treatment

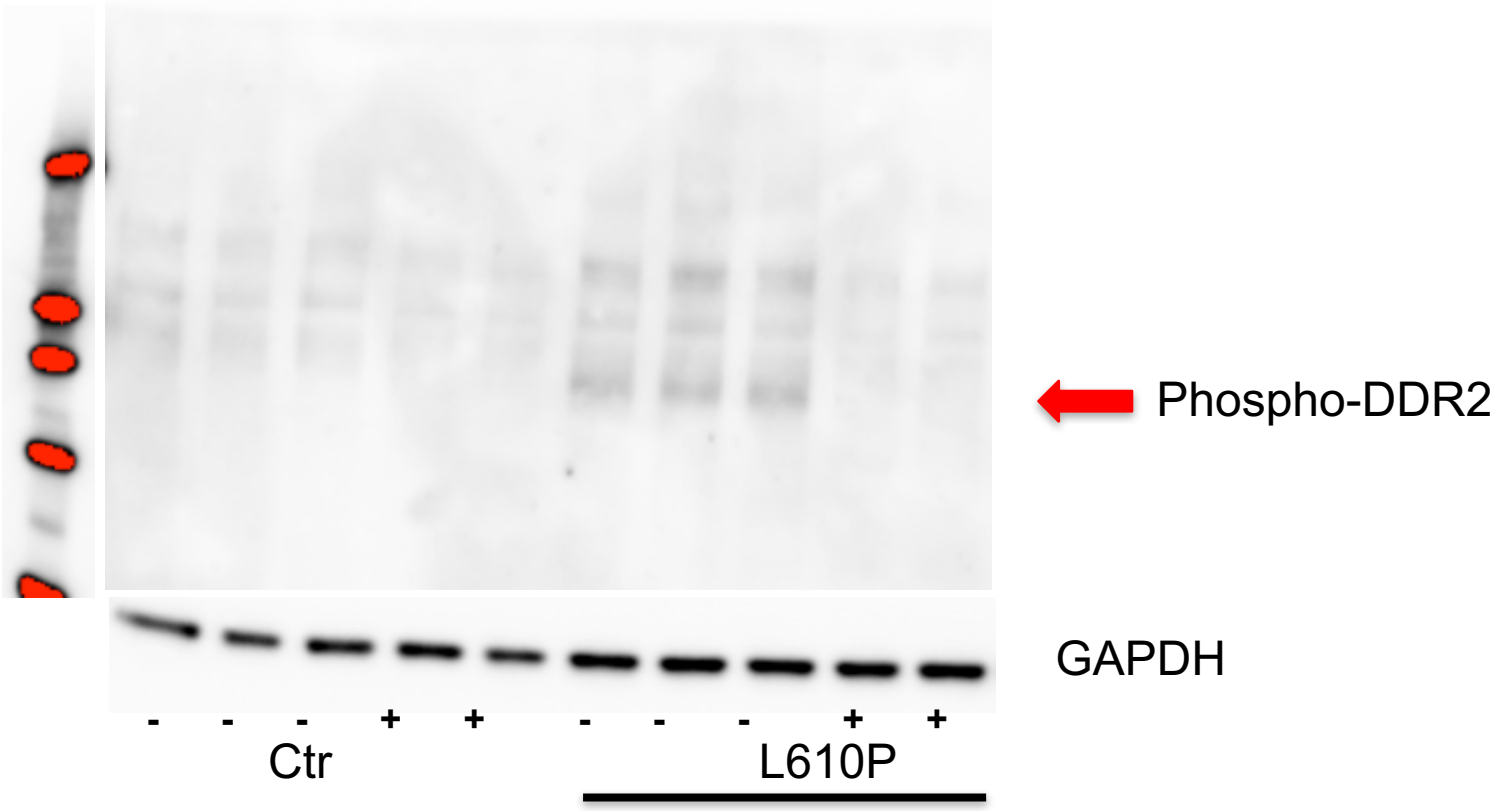

Immunoblot analysis of fibroblasts harboring the p.(Leu610Pro) substitution.
Cells serum-starved overnight were left untreated (-) or treated (+) with 0.1 μM dasatinib and harvested for immunoblot analysis after 6 hours. In treated fibroblasts with the p.(Leu610Pro) substitution, the band representing phospho-DDR2 (marked with a red arrow) disappears.

Figure S23: Phosho-DDR2 immunoblot results after dasatinib treatment

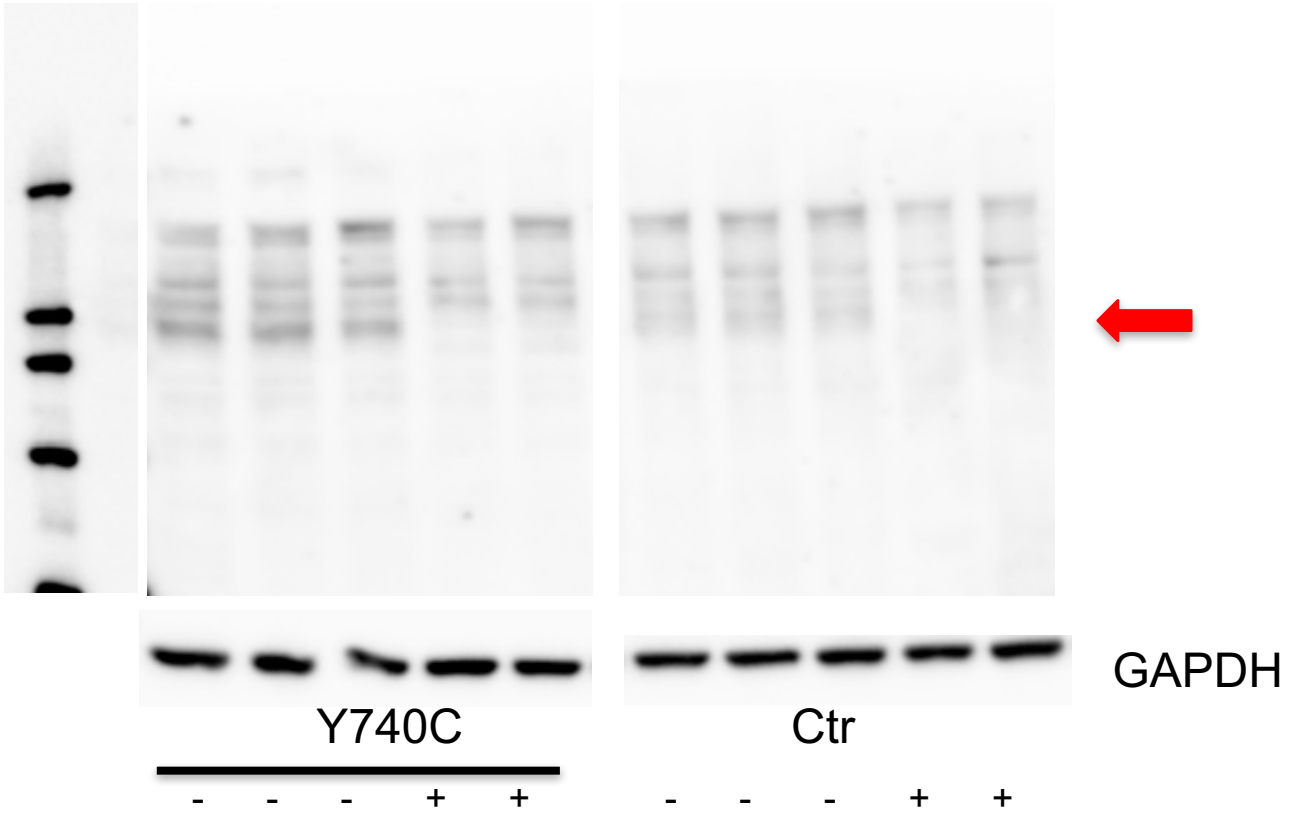

Immunoblot analysis of fibroblasts harboring the p.(Tyr740Cys) substitution.
Cells serum-starved overnight were left untreated (-) or treated (+) with 0.1 μM dasatinib and harvested for immunoblot analysis after 6 hours. In treated fibroblasts with the p.(Leu610Pro) substitution, the band representing phospho-DDR2 (marked with a red arrow) disappears.

Table S1: Overview of phenotypic features

	Indiv. 1 (age 57 y) Warburg et al. p.(Leu610Pro)	Indiv. 2 (age 58 y) Cinotti et al. p.(Tyr740Cys)	Indiv. 3 (age 31 y) Index mother p.(Tyr740Cys)	Indiv. 4 (age 8 y) Child of indiv. 3 p.(Tyr740Cys)	Indiv. 5 (age 3 y) Child of indiv. 3 p.(Tyr740Cys)	Indiv. 6 (age 35 y) Singleton indiv. p.(Leu610Pro)
Palpebral fissures	Narrow	Narrow	Normal	Narrow	-	Narrow
Cornea	BE: Advanced corneal vascularization	BE: Advanced corneal vascularization	RE: Advanced corneal vascularization	BE: Superior corneal vascular pannus	BE: Superior corneal vascular pannus	No abnormalities reported
Retina	Retinal dystrophy	Normal fundus	Normal fundus	-	-	-
Vision	BE: 2/60 - Light perception	RE: Light perception LE: 2-3/50	RE: Hand movement LE: 20/16	Normal	-	-
Facial features	Thin nose with small alae nasi Long face, small chin	Thin nose with small alae nasi	Thin nose Long face	Thin nose Long face	Thin nose Long face	Thin nose with small alae nasi
Oral cavity	High palate Abnormal teeth	Gingival hypertrophy Dental prostheses	Normal	-	-	High palate Dental crowding
Ears	Post. rotated ears Ear canal atresia Cholesteatoma Conduct. hearing loss	Post. rotated ears Normal hearing	Post. rotated ears Thin cartilage	Cholesteatoma Thin cartilage	-	Conductive hearing loss
Skin	Thin skin with little subcutaneous tissue	Hyperkeratotic, verrucoid and skin with multiple pigmented keloids	Thin skin with little subcutaneous tissue Linear keloid-like plaques Follicular hyperkeratosis	Thin skin with little subcutaneous tissue Papular rash on arms	Follicular hyperkeratosis	Thin skin with little subcutaneous tissue Angiodermatofibromas Lichenoid lesions Thick keloid-like scars
Joints	Contractures in hands and elbows Kyphosis	Contractures of phalanges, wrists and ankles	Contractures of phalanges and wrists Joint swellings	Contractures of phalanges Joint swellings	Contractures of phalanges Joint swellings	Contractures of phalanges Joint swellings
Hands and feet	Acro-osteolysis Chronic toe ulcers Loss of toenails	Acro-osteolysis Palmar fibrotic bands Loss of toenails	Acro-osteolysis Loss of toenails and toes Cutaneous fusions Sterile abcesses	Palmar fibrotic bands Bluish skin tumor on left foot sole	-	Chronic toe ulcers Loss of toes and forefoot tissue
Miscellaneous	Pneumothorax Hypogonadism Dysphagia	Gynecomastia Mitral valve insuff.	Hypothyroidism Large frontal sinuses	-	-	Pneumothorax Hypothyroidism Mitral valve insuff. Brain infarction Pyloric stenosis Chronic diverticulitis

Indiv. = individual, insuff. = insufficiency, BE = both eyes, RE = right eye, LE = left eye

Supplemental Methods

Exome sequencing of individuals 1, 2 and 6

For individuals 1 and 2, DNA was extracted from EDTA whole blood using QiaSymphony (Qiagen, Hilden, Germany). The DNA quality and quantity were evaluated with 1% SeaKem gel electrophoresis and NanoDrop spectroscopy (Thermo Fisher Scientific, Waltham, MA, USA), respectively. Library preparation for exome sequencing was performed using the NimbleGen SeqCap EZ MedExome Target Enrichment Kit (Roche Sequencing, Pleasanton, CA, cat.# 7676581001) and Kapa hyper Prep kit (Roche Sequencing, cat.# KK8504), according to the manufacturers recommendations. Eight individual samples were pooled and then paired-end sequenced on Illumina NextSeq500 using the NextSeq 500/550 v2 sequencing reagent kits (Illumina, San Diego, CA, cat.# FC-404-2002). Demultiplexing (bcl2fastq2-v2.16.0.10), trimming (Trimmomatic-0.33), alignment (bwa-0.7.12), realignment and variant calling (picard-tools-1.129 and GenomeAnalysisTK-3.3-0),[1] were performed in our default diagnostic pipeline, following the Broad recommended best practice guidelines.[2]

Filtering and variant annotation of these data were performed individually in Cartagenia Bench NGS module (Agilent Technologies, Santa Clara, CA), following our routine diagnostic procedure. In short, this involves two separate, but parallel branches of filtration depending on autosomal recessive or autosomal dominant inheritance. In the recessive branch, common variants with a frequency of ≥ 2% are filtered, while in the dominant branch common variants with a frequency of ≥ 0,1% are filtered. The source of common variants consisted of 1000 Genomes Phase1 release v3.20101123, 1000 Genomes Phase 3 release v5.20130502, NCBI ClinVar 20151102, dbSNP build 137 (verified only), ESP6500, ExAC release 0.3 and our own in-house generated variant frequency database based on exome sequencing of 800 individuals. Each source of common variants was queried individually.

Finally, we compared the variant lists of individuals 1 and 2, and made a list of all variants shared by these unrelated individuals. We then removed all variants previously classified as benign in our diagnostic pipeline, and all variants present in dbSNP build 137. Only four heterozygous missense variants remained, and they were in just two genes, *DDR2* and *MUC4*:

1) *DDR2*(NM_001014796.1) c.1829T>C, p.(Leu610Pro), and c.2219A>G, p.(Tyr740Cys).
2) *MUC4*(NM_018406.6) c.7571G>A, p.(Gly2524Asp), and c.14839G>A, p.(Ala4947Thr).

Both *DDR2* variants affected conserved nucleotides and amino acids, and both were

predicted to be detrimental by the following *in silico* prediction programs: PolyPhen2, MutationTester, SIFT and LRT. The CADD score (University of Washington, Hudson-Alpha Institute for Biotechnology, and Berlin Institute of Health) strongly suggested that both variants were unlikely chance findings, being 4.18 (raw score) and 30 (PHRED score) for p.(Leu610Pro), and 4.19 (raw score) and 31 (PHRED score) for p.(Tyr740Thr). In contrast, the two *MUC4* variants were located in non-conserved nucleotides and amino acids, and both were predicted to be benign/neutral or polymorphisms by the *in silico* tools mentioned above. Later, exome sequencing was also done in individual 6, and the same p.(Leu610Pro) variant was found as in individual 1. All variants were verified by Sanger sequencing.

Exome sequencing of individuals 3-5

Solution-hybridization exome capture was performed with the Nimblegen SeqCap EZ Library + UTR (Nimblegen/Roche Sequencing, Pleasanton, CA, USA), and exome sequencing was performed with the HiSeq 2500 sequencer (Illumina). Image analyses and base calling were performed using RTA 1.18.64 and Casava 1.8.2. Reads were aligned to the NCBI Genome browser reference genome GRCh37, hg19 with Novoalign (Novocraft Technologies, Selangor, Malaysia). Samples were sequenced to sufficient coverage such that at least 85% of the targeted exome was called with high-quality variant detection (reported as genotype at every callable position). Genotypes were called with only those sequence bases with Phred base qualities of at least Q20 via Most Probable Genotype[3] (MPG) and an MPG score of ≥10.

Patient 3 had three rare heretozygous *de novo* variants (*DDR2*, *TOM1*, *CNTRL*), but the only variant that segregated with the disease and was absent from population databases was the p.(Tyr740Cys) *DDR2* variant. This variant was inherited by two of her three children, patients 4 and 5.

ELISA analysis

Fibroblasts from patients 1 and 3, carrying the p.(Leu610Pro) and p.(Tyr740Cys) variant respectively, and control fibroblasts were obtained and cultured in Dulbecco`s modified Eagles` medium (DMEM) - high glucose (Lonza, Verviers, Belgium) supplemented with 10% fetal calf serum, penicillin/streptomycin and glutamine. When 80% confluent, new medium was added and the cells were harvested the following day in 1% NP-40 alternative, 20 mM Tris (pH 8.0), 137 mM NaCl, 10% Glycerol, 2 mM EDTA, 1 mM activated sodium orthovanadate, 10 μg/ml aprotinin and 10 μg/mL leupeptin. To measure phosphorylated DDR2, a DuoSet IC phospho-DDR2 kit was used (R&D Systems, Oxon, UK, cat.# DYC6170,) following the manufacturer's recommendations. A capture antibody that is specific for human DDR2 binds both phosphorylated and unphosphorylated DDR2 in this sandwich

ELISA. After washing, a HRP conjugated phosphorylated tyrosine antibody is used to detect only the phosphorylated receptor.

Western blot analysis

For Western blot analysis, cells were serum starved over-night, then lysed in 50 mM Tris-HCl, pH 7.5, containing 200 mM NaCl, 5 mM EDTA, 1% Igepal, 1 mM phenylmethylsulfonyl fluoride, complete protease inhibitor cocktail (Roche Diagnostics GmbH, Mannheim, Germany), 0.5% Tween, and 0.1 % SDS. Proteins were separated with a high-resolution gel system (4-12% NuPAGE Novex Bis-Tris Gel; Life technologies, Carlsbad, CA), transferred to nitrocellulose membranes (Bio-Rad, Hercules, CA) and incubated overnight at 4°C with antibodies, as described below at recommended dilutions. The membranes were washed and incubated with horseradish peroxidase-conjugated secondary antibodies from Cell Signaling Technology: anti-rabbit IgG (cat.#7074) and anti-mouse IgG (cat.#7076) for 1 hour at room temperature. Proteins were visualized using the Super Signal West Pico system alone or with added Super Signal West Femto Maximum Sensitivity Substrate (Thermo Fisher Scientific, Rockford, IL). A protein standard (MagicMark; Thermo Fisher Scientific) was used as a molecular weight marker. Chemiluminiscence was detected using the ChemiDoc Touch Imaging System (Biorad). To control for equal loading the membranes were blocked again and incubated overnight with anti-GAPDH primary antibody (cat.#G99545-Sigma-Aldrich, St. Louis, MO) and visualized as described above. HEK293 cells transiently transfected with DDR2 vector pMMLV[Exp]-hDDR2[NM_001014796.1]: IRES:Puro (VectorBuilder, Santa Clara, CA) was used as a positive control for phospho-DDR2 and total DDR2.

<u>Antibodies and conditions:</u>

Phospho-Tyr740DDR2 (cat.# MAB25382) and DDR2 (cat.#MAB2538) (R&D systems)
Concentration: 1/1000
Block: 5% Nonfat dry milk in Tris Buffered Saline with 0.1%Tween (TBST)
Short wash in TBST
Primary antibody: 1% Nonfat dry milk in TBST overnight
Wash 10 minutes with TBST x 3
Secondary antibody: 5% Nonfat dry milk in TBST
Was 10 minutes with TBST x 3

Phospho-Tyr542-PTPN11/SHP-2 (cat.#3751), PTPN11/SHP-2 (cat.#3397), phospho-Ser473-AKT (cat.#4060), AKT (cat.#4691), phospho-Thr202/Tyr204-MAPK3/ERK1 (cat.#4370), MAPK3/ERK1 (cat.#4695), phospho-Tyr416-SRC (cat.#69439), Tyr416-SRC (cat.#2102), phospho-Tyr527-SRC (cat.#2105), Tyr527-SRC (cat.#2107), SRC (cat.#2123), phospho-Tyr70-STAT1 (cat.#7649)
Concentration: 1/1000

Block: 5% Nonfat dry milk, 1% BSA, 1% Glycine in Phosphate Buffered Saline with 0.5% Tween (PBST)
Primary antibody: 1% Nonfat dry milk, 1% BSA, 1% Glycine in PBST overnight
Wash 15 minutes with PBST x 3
Secondary antibody: 1% Nonfat dry milk in PBST
Was 15 minutes with PBS x 3

Phospho-Tyr580-PTPN11/SHP-2 (cat.#3703)
Concentration: 1/1000
Block: 5% Nonfat dry milk in Tris Buffered Saline with 0.1%Tween (TBST)
Wash 5 minutes with TBST x2
Primary antibody: 5% BSA in TBST overnight
Wash 5 minutes with TBST x 3
Secondary antibody: 5% Nonfat dry milk in TBST
Wash 5 minutes with TBST x 3

ClinVar registration

Both DDR2 variants have been registered in NCBI's ClinVar database:
p.(Leu610Pro) under submission number SUB4623779
p.(Tyr740Cys) under submission number SUB4624426

References

1. McKenna A, Hanna M, Banks E, et al. The Genome Analysis Toolkit: a MapReduce framework for analyzing next-generation DNA sequencing data. Genome Res 2010;20:1297-303.

2. Van der Auwera GA, Carneiro MO, Hartl C, et al. From FastQ data to high confidence variant calls: the Genome Analysis Toolkit best practices pipeline. Curr Protoc Bioinformatics 2013;43:11 10 1-33.

3. Johnston JJ, Sanchez-Contreras MY, Keppler-Noreuil KM, et al. A Point Mutation in PDGFRB Causes Autosomal-Dominant Penttinen Syndrome. Am J Hum Genet 2015;97:465-74.